ALGERIAN PEOPLE'S DEMOCRATIC REPUBLIC
MINISTRY OF HIGHER EDUCATION AND SCIENTIFIC RESEARCH

University of Hamma Lakhdar EL-OUED Faculty of Science and Technology

Department of Process Engineering

Master Thesis

In order to obtain the diploma of

Academic Master

Field: Process Engineering

Specialty: Chemical Engineering

Prepared by students:

Memmadi Mehrez, Chergui Elhadi

The topic

Applications of Iron Oxide Nanoparticles in Food Safety Control

Defended on: 03/06/2024

In front of the jury of :

President	Dr. Abderrhmane Bouafia	Associate Professors, Grade B. Univ. Eloued
Examiner	Dr. Moussa Boudiaf	Associate Professors, Grade A. Univ. Eloued
Supervisor	Dr. Kaouthar Ahmouda	Associate Professors, Grade A. Univ. Eloued

Academic year: 2023/2024

Acknowledgement

First and foremost, we extend our deepest gratitude to **ALLAH** for His guidance and mercy throughout this work. His inspiration and support have been instrumental in helping us take the right steps and make right decisions. Without His blessings, this work would not have been possible.

This work was carried out at the Renewable Energy Research Unit in Arid Zones, University El Oued, directed by **PROFESSOR OUCIF KHALED**, to whom we express our deep respect and we thank you for the help and support he gave us.

We would like to thank our supervisor **DR. AHMOUDA KAOUTHAR**, a respected lecturer at the Faculty of Technological Sciences at the University of El Oued, for her invaluable guidance, expertise and support throughout the entire research process. Her insightful comments and constructive criticism have greatly shaped the development of this Thesis.

We also thank the members of the jury for agreeing to evaluate our work.

We would also like to express our sincere thanks to the laboratory staff for their help.

We would also like to particularly thank **MR. ALI TALIBA**, engineer from the VTRS laboratory.

We would also like to thank the team of the Renewable Energy Research Unit in Arid Zones and more particularly **MR. IBRAHIM CHERIET** and **MR. NANI SADEK**, laboratory engineer.

We extend our thanks to our friend's class 2024 who shared the burden of this research.

A big thank you to everyone who participated in the success of this research, whether directly or indirectly.

Mehrez end Elhadi

DEDICATION

I am dedicating this work to people who have meant and will mean so much to me.

To my dear parents, my father **MOHAMED** and my mother **KHADIJA** who enlightened me through their by their exemplary dedication and the enormous sacrifices they made .great support and encouragement to me during my studies and who always loved to see me succeed. I thank them for everything they have done to me.

To my maternal aunt **NAIMA** who was more than a real maternal aunt

To my adorable sisters: **DJAMILA** and **NARDJESS** for who were the supports, the guides and the lessors, they never left me in need of anything.

To my dear brothers: **AHMED** and **RAAFET** for always being there for me.

.To the youngest of family: **GHAITH** whom gave me happiness in its most beautiful qualities

To all our friends in whom we have always found comfort and support.

MEHREZ

DEDICATION

To my dear father, whose soul left us and left in our hearts nostalgia and the desire to meet again

and to my dear mother, who is our constant wishes and the light of our path

to my dear brothers and sisters who shared every moment of this beautiful journey with me

as well as my beloved wife and dear children who fill my life with happiness and love

To all my family and friends who share my joy and sorrow, I dedicate this letter as a profound testimony of my love and gratitude to you all.

ELHADI CHERGUI

Abstract

This work investigates the study of colorimetric detection of ascorbic acid which is a spoilage compound in food by Mo (VI)/IONPs. This work aims to develop a biosensor for the colorimetric detection of this spoilage compound (ascorbic acid) by four different biosensors which are: Mo (VI)/ARM-Fe_3O_4, Mo (VI)/ROS-Fe_3O_4, Mo (VI)/MAT-Fe_3O_4, and Mo (VI)/JUN-Fe_3O_4. The detection of ascorbic acid contributes to controlling food security. The experiments were conducted under 95 °C for 1 h of oxidation reaction of ascorbic acid by ammonium molybdate. The absorbances of blue complex formed by the oxidation of ascorbic acid were measured at 820 nm. The impact of pH solution was studied in the range of 1-5. The findings showed that pH =3 is the optimal. Furthermore, ascorbic acid was highly detected by Mo (VI)/ARM-Fe_3O_4, then Mo (VI)/ROS-Fe_3O_4, next Mo (VI)/MAT-Fe_3O_4, and finally Mo (VI)/JUN-Fe_3O_4 biosensors. LOD and LOQ were also calculated, where obtained results of Mo (VI)/ARM-Fe_3O_4, Mo (VI)/ROS-Fe_3O_4, Mo (VI)/MAT-Fe_3O_4, and Mo (VI)/JUN-Fe_3O_4 NPs are found to be LOD: 0.47, 0.43, 0.37, and 0.32 mM, and LOQ: 1.566, 1.4315, 1.2333 and1.0666 mM. The interference of $Cacl_2$, $CuCl_2$, and KCl was analyzed. The obtained results showed that these interferents have not a significant interference on ascorbic acid detection. This leads to declare that Mo (VI)/ARM-Fe_3O_4 biosensor is simple, rapid, and highly sensitive for detecting ascorbic acid.

Keywords: iron oxide nanoparticles, food security, colorimetric method, ascorbic acid, spoilage compound

ملخص

يهدف هذا العمل إلى دراسة الكشف اللوني لحمض الأسكوربيك وهو مركب مفسد في الأغذية بواسطة Mo(VI)/ IONPs يهدف هذا العمل إلى تطوير حساس حيوي للكشف اللوني لمركب التلف (حمض الأسكوربيك) بواسطة أربعة حساسات حيوية مختلفة وهي $Mo(VI)/MAT-Fe_3O_4$, $Mo(VI)/ROS-Fe_3O_4$, $Mo(VI)/ARM-Fe_3O_4$ و $Mo(VI)/JUN-Fe_3O_4$. يساهم الكشف عن حمض الأسكوربيك في التحكم في سلامة الأغذية. أجريت التجارب تحت درجة حرارة 95 درجة مئوية لمدة ساعة واحدة من تفاعل أكسدة حمض الأسكوربيك بواسطة موليبدات الأمونيوم. تم قياس امتصاصية المركب الأزرق المتكون من أكسدة حمض الأسكوربيك عند 820 نانومتر. تمت دراسة تأثير محلول الأس الهيدروجيني في حدود 1–5. وأظهرت النتائج أن الرقم الهيدروجيني 3 هو الأمثل. علاوة على ذلك، تم اكتشاف حمض الأسكوربيك بشكل كبير بواسطة أجهزة الاستشعار $Mo(VI)/ARM-Fe_3O_4$ ثم $Mo(VI)/ROS-Fe_3O_4$ ثم Mo (VI)/$MAT-Fe_3O_4$) وأخيرًا $Mo(VI)/JUN-Fe_3O_4$. تم أيضًا حساب LOD وLOQ، حيث تم العثور على نتائج $Mo(VI)/ARM-Fe_3O_4$, $Mo(VI)/ROS-Fe_3O_4$, Mo (VI)/$MAT-Fe_3O_4$ و Mo (VI)/$JUN-Fe_3O_4$ NPs أن يكون LOD = 0.32, 0.37, 0.43 , 0.47 mM و LOQ = 1.66, 1.43, 1.56, 1.23 mM. تم تحليل تداخل $CaCl_2$ و $CuCl_2$ و KCl. أظهرت النتائج المتحصل عليها أن هذه المتداخلات ليس لها تداخل معنوي في الكشف عن حمض الأسكوربيك. يؤدي هذا إلى الإعلان عن أن جهاز الاستشعار الحيوي Mo(VI) /$ARM-Fe_3O_4$ بسيط وسريع وحساس للغاية للكشف عن حمض الأسكوربيك.

الكلمات المفتاحية: جزيئات أكسيد الحديد النانوية، الأمن الغذائي، الطريقة اللونية، حامض الاسكوربيك، مركب التلف.

List of contents

List of figures

List of tables

Abbreviation list

NPs	Nanoparticles
IONPs	Iron oxide
FTIR	Transform infrared spectroscopy Fourier
XRD	X-ray diffraction
SEM	Scanning electron microscopy
µm	Micrometer
UV-Vis	Ultraviolet and visible
Nm	Nanometers
SI	International unit
D	Dimensional
%	Percentage
Ph	potential of hydrogen
Fe_3O_4	Iron oxide
γ-Fe_2O_3	Magnetite
α-Fe_2O_3	Hematite
Ml	Milliliter
Mm	Millimol
Mg	Milligram
LOQ	Limit of quantification
LOD	Limit of detection
λ	wavelength
D	interticular distance
Θ	Angle
n	An integer
E_0	Standard Electrode Potential

GENERAL INTRODUCTION

General introduction

Food security is a critical global issue, focusing on ensuring that all people have access to sufficient, safe, and nutritious food to maintain a healthy life[1]. This encompasses not only the availability of food but also its quality and safety[2]. Spoilage compounds, which can degrade the nutritional value and safety of food products, pose a significant challenge to food security. Effective detection and control of these compounds are essential to prevent foodborne illnesses and economic losses[3, 4].

Innovative technologies and methodologies are continuously being developed to enhance the monitoring and management of food quality. One such approach is the use of iron oxide nanoparticles as biosensors for detecting ascorbic acid, a common spoilage compound[5, 6]. These nanoparticles possess unique magnetic and optical properties that make them ideal for sensitive and accurate biosensing applications[7]. In colorimetric assays, they interact with ascorbic acid, producing a measurable color change that indicates its presence and concentration. This method provides a rapid, reliable, and cost-effective means of monitoring ascorbic acid levels in food products, thereby ensuring their quality and safety[8]. By incorporating such advanced biosensing technologies, the food industry can better control spoilage compounds, contributing to enhanced food security and consumer protection[9].

Vitamin C (ascorbic acid) is essential for human health, contributing to the immune system, collagen formation, and iron absorption. Its detection is crucial for maintaining food safety, quality, and shelf life[6, 10]. Colorimetric detection methods, which rely on a chemical reaction that changes color in the presence of vitamin C, offer a simple and effective tool for this purpose[11]. Such methods can be used in laboratories and at home to monitor vitamin C levels in foods and nutritional supplements, providing an effective and inexpensive way to ensure appropriate concentrations[12]. The aim of our work is to develop four different biosensors: Mo(VI)/ARM-Fe_3O_4, Mo(VI)/ROS-Fe_3O_4, Mo(VI)/MAT- Fe_3O_4, and Mo(VI)/JUN- Fe_3O_4 for detecting ascorbic acid. The development of these biosensors contributes to controlling food security.

This thesis is divided into two parts:

Theoretical part: includes chapter I and II:

Chapter I: Focuses on general concepts in nanotechnology, as well as a theoretical study of iron oxide nanoparticles in terms of their structure, properties, and applications, in addition to methods of preparation and characterization.

Chapter II: Includes generalities about food security and types of methods for detecting ascorbic acid.

Practical part: includes chapter III:

Chapter III: Presents the materials used and the method applied to greenly synthesised iron oxide nanoparticles and their characterisation by technical analysis. Moreover, the colorimetric detection of ascorbic acid using the Mo (VI)/Magnetite NPs biosensors is detailed. Finally, presentation of obtained the results and discussion.

This thesis is concluded by a general conclusion that summarizes obtained results.

CHAPTER I: LITERATURE REVIEW

I-1- Introduction:

The science of nanotechnology, which operates at a scale of one millionth of a millimeter (1-100 nm), focuses on phenomena unique to this size range. By manipulating materials at the nanoscale, nanotechnology reveals unique physical, chemical, and biological properties, enabling the creation of entirely new products[13, 14].

Iron oxides are very common in nature. They are found in the earth's crust (rock, ore), in water (erosion by water, rivers, etc.) and in biological organisms (human body, animals, plants)[15]. They were used very early by humans: already, in prehistoric times, cave paintings contained iron oxide pigments. Then, they were used in many other fields (physics-chemistry-biology). Iron compounds have many applications. Pigments containing iron oxide are used in coatings and as colorants in ceramics, glass, plastics, rubber, etc [16, 17].

I-2- Iron oxide (IONPs): Definition, types, and applications

Iron (Fe) is a chemical element with atomic number 26, and by mass it is the most abundant metal on the planet. Iron can form several oxides: iron oxide wustite (FeO), which is very rare; Hematite (α-Fe_2O_3), maghemite (γ-Fe_2O_3), and ferric iron oxide (Fe_3O_4), all of which exhibit ferromagnetic properties and are widely distributed in nature, but can also be synthesized in the laboratory[18, 19].

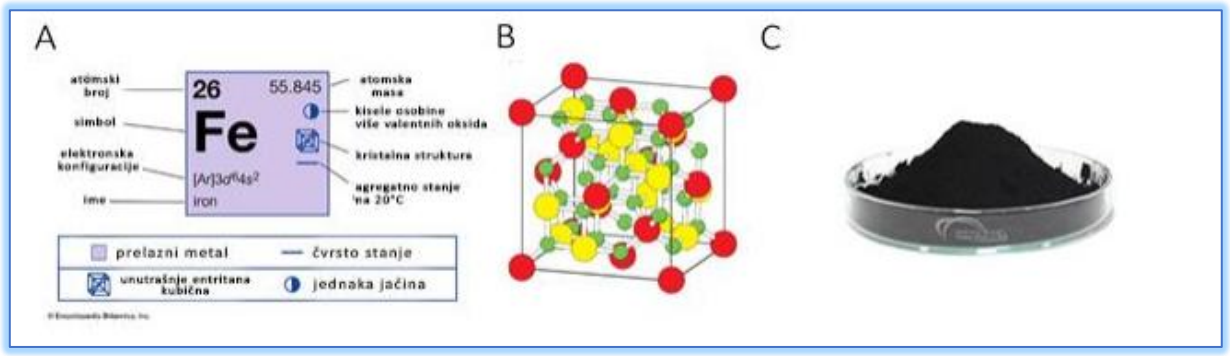

Figure I.1: The structural properties of IONPs[19].

I-2-1- Hematite (α-Fe_2O_3):

Hematite stands out as the most stable form of iron oxides due to its high level of oxidation. Its name, derived from the Latin "haematites," and ultimately from the Greek word "αιματ ιτηζ," reflects its characteristic blood-red hue when in powdered form. Hematite garners significant interest due to its diverse range of applications, including its use in synthesizing ferrites, acting as catalysts, serving as dyes, and providing protection against[20].

I-2-2- Magnetite (γ-Fe_2O_3):

Magnetite, with the chemical formula Fe3O4, possesses the most significant magnetic properties among the three main iron oxides. Also known as ferrous ferrite, black iron oxide, loadstone, or magnetic iron ore, magnetite is renowned for its strong magnetic characteristics. Maghemite (γ-Fe2O3), another type of iron oxide, is a product of weathering that results from the exposure of magnetite to water or atmospheric gases [21].

I-2-3- Maghemite (γ-Fe_2O_3):

Maghemite (γ-Fe2O3), the third type of iron oxide, forms as a weathering product of magnetite when it comes into contact with water or atmospheric gases[22].

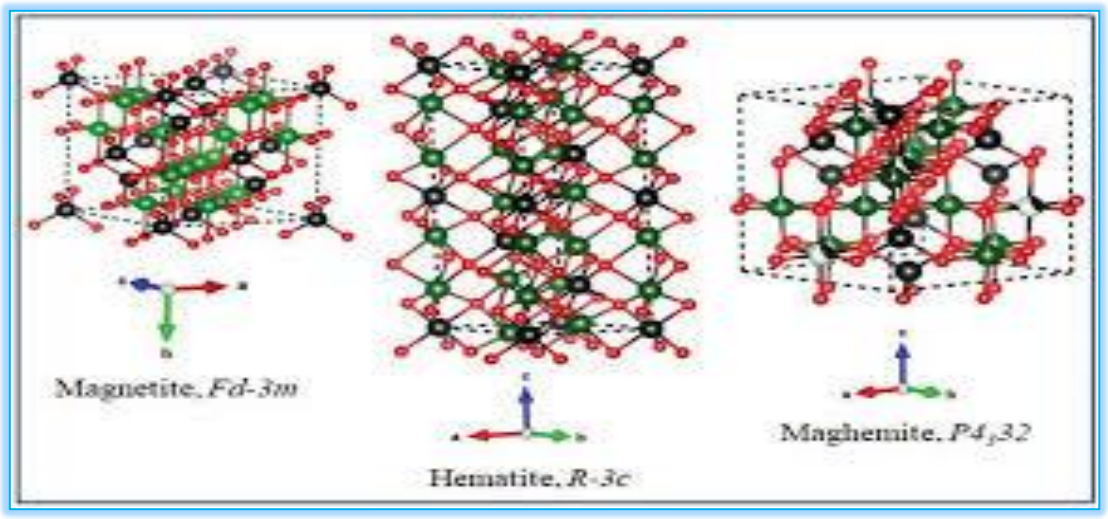

Figure I.2: Crystal Structures of Hematite, Magnetite, and Maghemite[23].

I-3- Properties of IONPs:

Iron oxide nanoparticles enable the creation of new materials that involve manipulating and creating molecules according to precise properties, while also functioning more effectively and being able to perform new roles. This is because different physical properties distinguish nanoparticles from larger materials. It is these properties that have greatly fuelled interest in its potential use. Due to their small size, nanoparticles have a very large surface area to volume ratio [24-26].

I-4- Classification of IONPs in terms of dimensions:

I-4-1- Zero-dimensional nanoparticles:

IONPs were categorized as 0-dimensional (0D) are among the most prevalent types of nanomaterials. These particles exhibit a point-like structure and typically have dimensions smaller than 100 nm. Common examples in this category include quantum dots, hollow spheres, and nano lenses[27].

I-4-2- One-dimensional nanoparticles:

IONPs with one dimension (1D) exceeding the nanoscale, while the other dimensions remain within the nano range, are referred to as one-dimensional nanoparticles. Common examples in this category include nanofibers, nanotubes, and nanorods[28].

I-4-3- Two-dimensional nanoparticles:

Two-dimensional (2D) IONPs are those with two dimensions exceeding the nanoscale, typically exhibiting plate-like structures. Examples of such materials include nanofilms, nanolayers, and nanocoatings [29].

I-4-4- Three-dimensional nanoparticles:

IONPs in three dimensions (3D) possess dimensions that exceed the nanoscale in all three directions. These structures are constructed by assembling nanoscale particles to create three-dimensional nanomaterials. Examples of such structures include nanocomposites, clusters of nanofibers, and multi-layered nanomaterials [30].

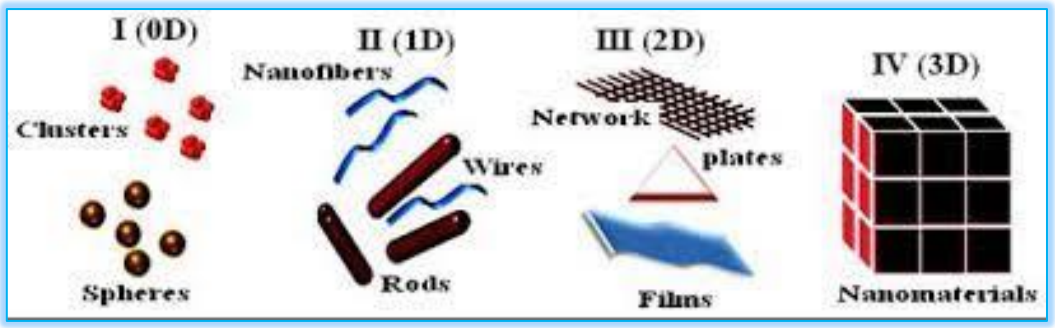

Figure I.3: Classification of various nanoparticles in terms of dimensions and shapes[31].

I-5- Synthesis of IONPs:

During the last decade of the twentieth century, research in the field of materials science focused on nanoparticles. Interest in nanoparticles has been driven by advances in preparation methods and the structural control and properties of new materials. Nanoparticles are frequently prepared by two methods[32, 33]:

I-5-1- Physical and chemical methods for synthesizing IONPs:

I-5-1-1- Inert gas condensation:

This method is one of the primitive methods for NP synthesis that uses inert gases (e.g. He or Ar) and liquid nitrogen-cooled substrate support for NP preparation. The evaporated materials are transported with inert gases and condensed on the substrate fixed with liquid nitrogen[34].

I-5-1-2- Physical vapor deposition:

This method is a collective set of processes commonly used to produce NPs and to deposit thin layers of material, typically on the order of a few nanometers to several micrometres. PVD is an environmentally friendly vacuum deposition technique consisting of three fundamental steps: (1) vaporization of the material from a solid source, (2) transport of the vaporized material, (3) nucleation and growth to generate thin films and NPs[35].

I-5-1-3- Laser ablation:

This method involves removing material from a solid surface by irradiation with a laser beam. The material is heated by the absorbed laser energy and evaporates or sublimes at low laser flux. At higher flux, the material is converted to plasma. The amount of material removed by a single laser

pulse and the depth over which the laser energy is absorbed depends on the optical properties of the material and the wavelength of the laser. Carbon nanotubes can be produced by this method[36, 37].

I-5-1-4- Sol-gel method:

This method includes two main stages: “sol” and “gel”. A “sol” is a colloidal suspension of solid particles in a liquid, while a “gel” is a substance containing liquid polymers. This process involves the creation of “sols” in the liquid, creating a network of discrete molecules or network polymers through the association of sol particles. In more detail, the process begins with preparing a solution containing solutes that will later turn into solid particles. As the process progresses, chemical reactions occur that lead to the formation of nanoparticles in the liquid. Over time, these particles bond together to form a three-dimensional network, forming the gel. This method can be used to prepare a wide range of nanomaterials, including metal oxides, glassy materials, and ceramic materials[38, 39].

I-5-1-5- Hydrothermal synthesis:

Is a method used to manufacture nanoparticles of metal oxides, iron oxide, and lithium iron phosphate by controlling the properties of the particles by modifying the properties of near-critical or supercritical water using different pressure and temperature conditions. This method can be performed in two types of systems: batch hydrothermal process or continuous hydrothermal process. The first system (batch hydrothermal process) is able to achieve a system containing the desired deposition stages, while the second (continuous hydrothermal process) has a higher reaction speed in a shorter period of time[40].

I-5-2- Biological methods:

I-5-2-1- Synthesis by microorganisms:

Synthesis of nanoparticles using green nanotechnology is emerging as a cleaner, economical, eco-friendly, stable, non-toxic and biocompatible method compared to conventional physical and chemical methods. Green and synthesized nanoparticles are used globally in the areas of food industry, pharmaceuticals, personal care products sector, biomedical engineering and microbial nanotechnology. Plant extracts and microorganisms such as bacteria, yeast, algae, fungi and cyanobacteria are the most versatile "nanobiofactories" that have been studied for synthesis of metal nanoparticles [41-44].

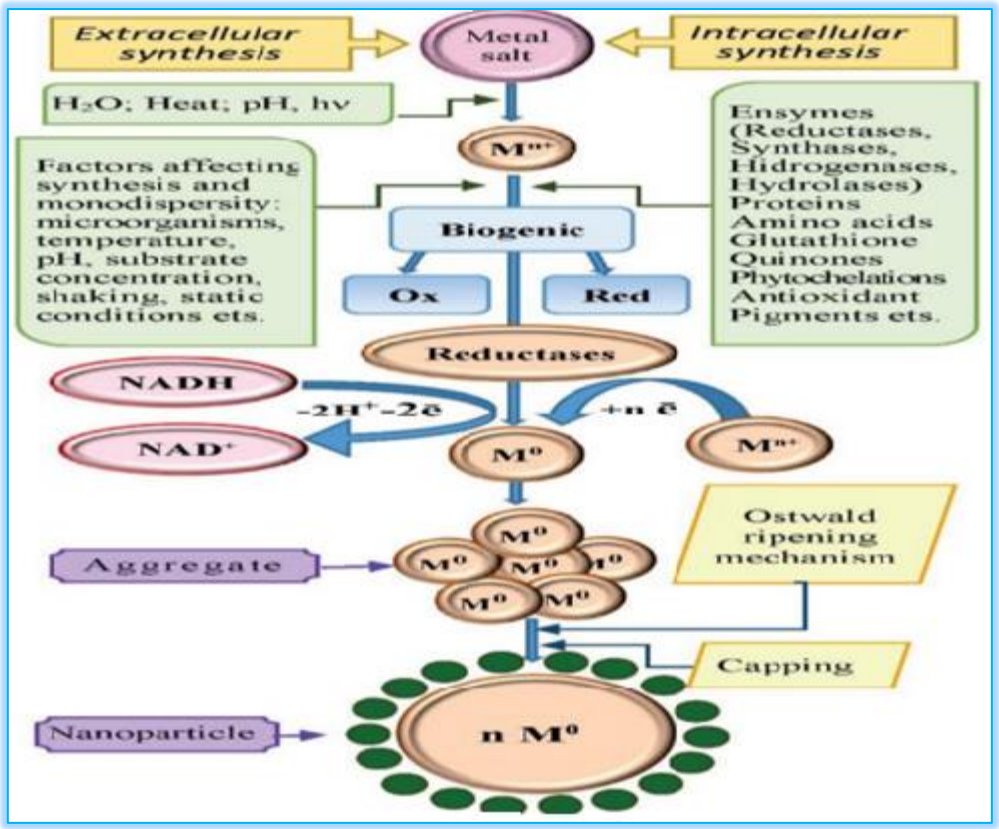

Figure I.4: Synthesis by microorganisms[41].

I-5-2-2- Green Synthesis:

Plants contain a wide range of bioactive compounds, including alkaloids, flavonoids, terpenoids, and steroids, which act as reducing agents in nanoparticle biosynthesis. Recently, several valuable desert plants have been used to make different types of nanoparticles. Various plant parts such as fruit, leaf, stem, root have been widely used for green synthesis of nanoparticles due to the excellent phytochemicals they produce. For nanoparticle synthesis, the part of the plant that is to be used in synthesis can be washed and boiled with distilled water. After extraction and filtration, the respective solutions to the nanoparticles that we want to synthesize are added. A color change is observed, revealing the formation of nanoparticles[45, 46].

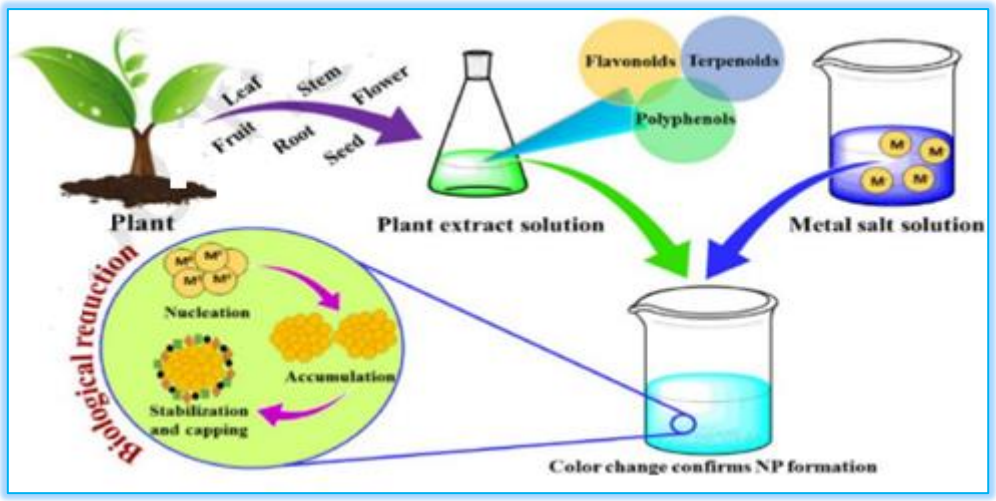

Figure I.5: Synthesis of nanoparticles (NPs) from the plant [47].

I-6- Applications of IONPs:

Iron oxide nanoparticles are typically applied in several applications include industrial, medicinal, and energy uses. These include more sustainable building materials, therapeutic drug delivery, and higher-density hydrogen fuel cells that are environmentally friendly. Since nanoparticles and nano devices are very versatile through modification of their physicochemical properties, they have found uses in nanoscale electronics, cancer treatments, vaccines, battery cells, etc. hydrogen fuel and nanographene batteries. The use of smaller sized materials allows adjustment of molecules and substances at the nanoscale, which can further improve the mechanical properties of materials or provide access to areas of the body less physically accessible[18, 48-50].

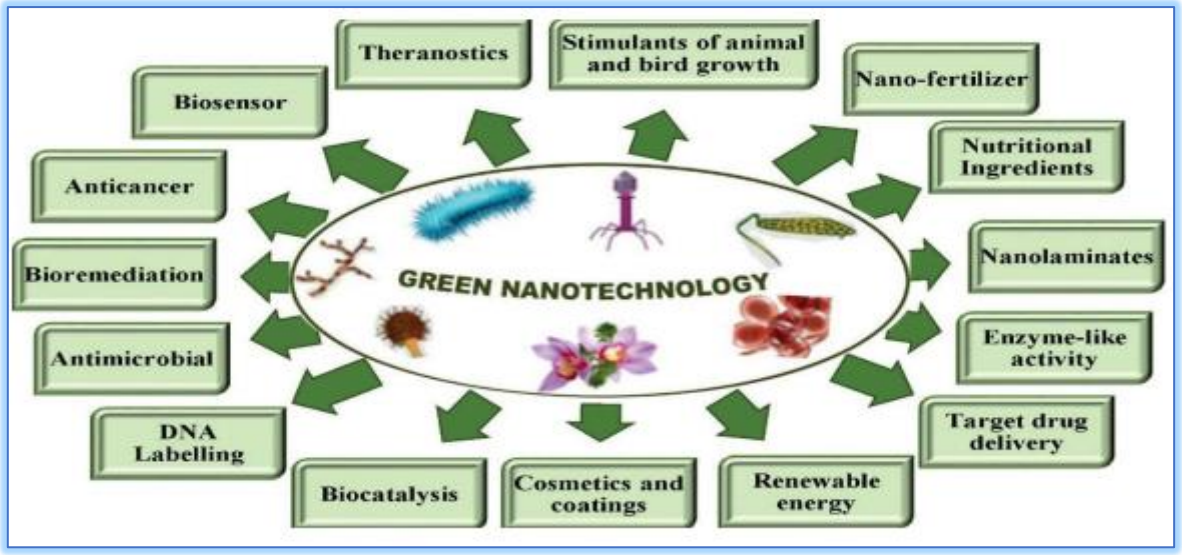

Figure I.6: Biosynthesized nanoparticles pave the way for various applications of nanotechnology[51].

I-6-1- Chemistry:

I-6-1-1- Catalysis:

Chemical catalysis is particularly beneficial for nanoparticles, due to their large surface-to-quantum ratio. Potential applications of nanoparticles in catalysis range from fuel cells to catalytic converters and photocatalysts. The importance of catalysis also appears in the production of chemicals[52, 53].

I-6-2- Biosensors

Through efficient and sustainable means, a complex set of technical and scientific challenges within the food industry and biological processes to produce safe and high-quality food can be solved using nanotechnology. Identification of bacteria and monitoring of food quality using biosensors; efficient, intelligent and active food packaging systems; Nanoencapsulation of bioactive food compounds are some examples of the emerging applications of nanotechnology for the food industry[9, 54, 55].

Iron oxide nanoparticles can be applied to food production, processing, safety and packaging[56]. A nanocomposite coating process could improve food packaging by injecting antimicrobial agents directly onto the surface of the coating film. Nanocomposites could increase or decrease the gas

permeability of different fillers depending on the needs of different products. They can also improve the mechanical strength and heat resistance properties and reduce the oxygen transmission rate. The research focuses on the application of nanotechnology to the detection of chemical and biological substances in foods [57-59].

I-7- Characterization technics used for characterizing IONPs:

In the present work, UV-Vis spectroscopy, X-ray diffraction (XRD), scanning electron microscopy (SEM), and Fourier Transform Infrared Spectroscopy (FT-IR) techniques have been used for the characterization.

I-7-1 Structural properties:

I-7-1-1- X-ray diffraction (XRD)

X-rays are electromagnetic radiation whose wavelength is between 0.01 and 10°A. This non-destructive technique is the most useful and widespread for identifying the nature and structure of crystallized products. In addition, X-ray diffraction provides access to physical information about crystals, notably their size and orientation[60, 61].

- **Principle**

This technique is based on the interactions of the crystal structure of a sample with short-wavelength monochromatic radiation. When the X-rays reach the reticular planes of the crystal lattices, either they come into contact with the electronic clouds of the atoms constituting this plane, in this case the obstacle and can continue to the second plane to be partially reflected again. These planes are separated by characteristic distances which depend on the nature of the material analyzed (reticular distances). The interference of the rays will be alternately constructive or destructive. The directions in which interference is constructive, called diffraction peaks, can be determined by Bragg's law [62, 63].

- **Bragg's law:**

When a crystalline species is irradiated with X-ray radiation of wavelength λ at an incidence θ, the radiation is diffracted if Bragg's law is verified [64]:

$$n\,\lambda = 2\,d\,sin\,\Theta$$

Were,

n is an integer which represents the order of reflection.

λ is the wavelength of X-rays.

d is the interticular distance.

θ is the angle of incidence of the X-rays

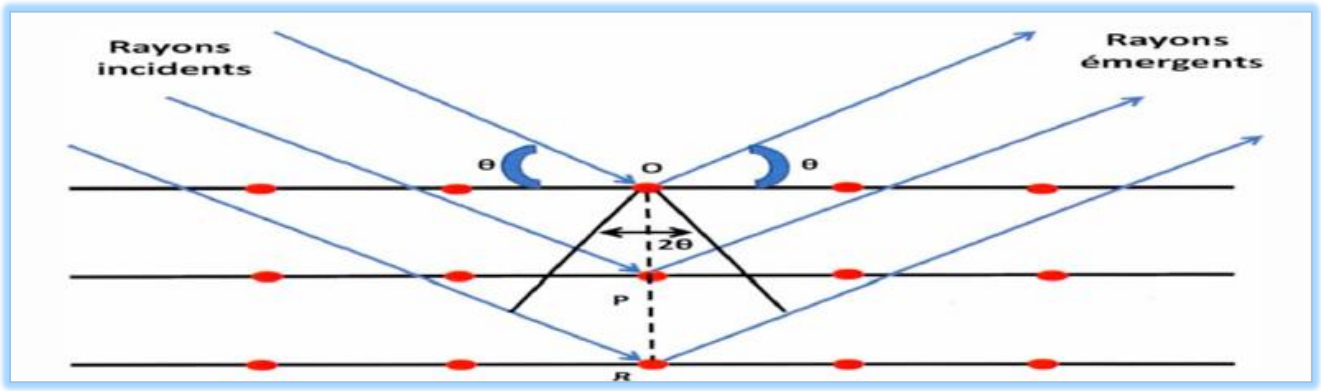

Figure I.7 : X-ray diffraction during interaction with materials[61].

In general, the study of the diffractogram makes it possible to identify a large number of information such as the orientation of a single crystal, the structural properties and the size and shape of the samples.

I-7-1-2- Scanning electron microscopy (SEM):

Scanning electron microscopy (SEM) or Scanning Electron Microscopy (SEM) is a technique that allows the observation of the surface morphology of a solid material. This technique therefore offers several advantages in morphological and dimensional analysis [65, 66].

➢ Principle

Scanning electron microscopy is a technique using electron-matter interactions. SEM provides images of the surface in relation to the mode of electron diffusion by the sample. These images are formed mainly using surface electronic emissions (secondary electrons and backscattered electrons).

The interaction between the electron beam of energy E_0 (the primary electrons) and the sample generates low energy electrons called “secondary electrons”. The latter are then accelerated towards a detector whose role is to amplify the electrical signal received (at each point, the intensity is converted into an electrical signal)[67] .

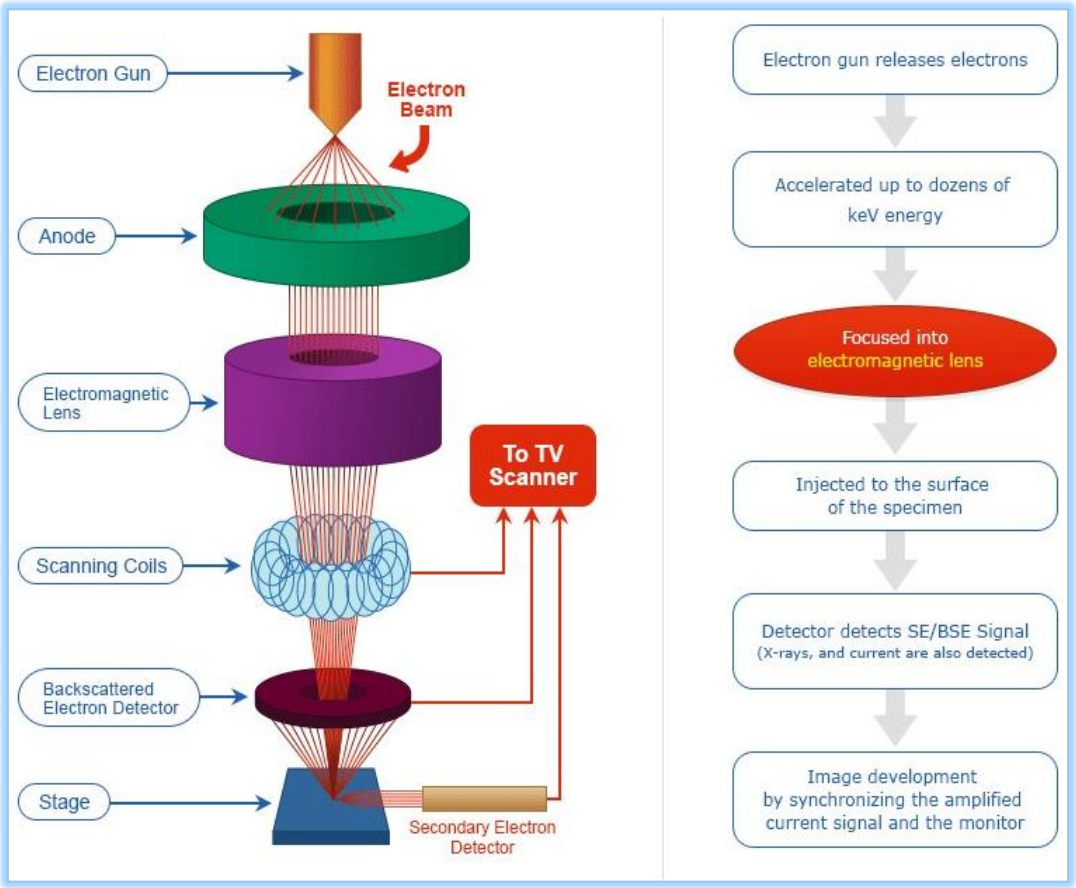

Figure I.8 : Schematic illustration scanning electron microscope[68].

I-7-1-3- FT-IR Spectroscopy:

FT-IR spectroscopy is a technique that allows information about different functional groups to be obtained from peak positions in the spectrum. Information on the identification and stabilization of nanoparticles can also be deduced from this analysis[71].

- **Principle:**

The principle of FTIR is based on the absorption of single or double beam infrared radiation by the sample to be analyzed. It allows, via the detection of vibration frequencies characteristic of chemical bonds, to carry out the analysis of the chemical functions present in the material.

The infrared beam is directed towards the Michelson interferometer which will modulate each wavelength of the beam at a different frequency. In the latter, the incident light beam is separated in two by a separator. These two parts will be reflected on mirrors, one of which is fixed and the other mobile. When the two beams recombine, destructive or constructive interference appears depending on the position of the moving mirror. The modulated beam is then reflected from the two mirrors towards the sample, where absorptions occur. The beam then arrives at the detector to be transformed into an electrical signal[71, 72].

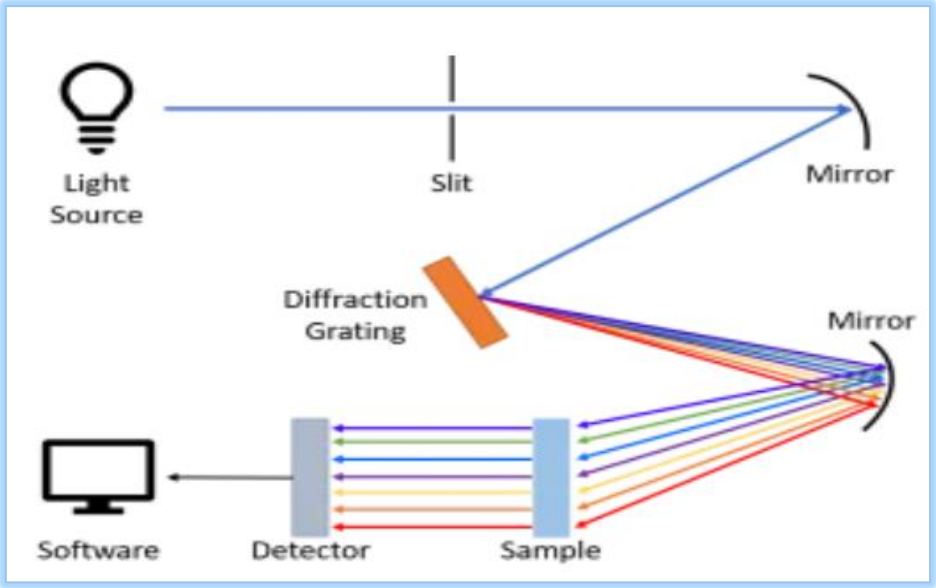

Figure I.9 : Principle of Operation of the FT-IR Spectrometer[71].

I-7-1-4- UV-Visible absorption spectroscopy:

UV-visible absorption spectroscopy is a very common characterization method in laboratories. It is based on the property of matter and more particularly certain materials, to absorb certain wavelengths of the UV Visible spectrum, where the absorbed energy causes disturbances in the electronic structure of atoms, ions or molecules[73].

➢ **Principle:**

The principle of this technique is based on light-matter interaction in the wavelength range between 180 and 1100 nm.

She is interested in electronic transitions from the ground state (σ, p or π) to an excited state (anti-bonding σ* or π*) caused by the absorption of light. It consists of measuring the attenuation of incident radiation of intensity I_0 as a function of the wavelength, when it passes through a homogeneous medium of thickness L[74].

The intensity of the transmitted radiation I is given by the law Beer-Lambert according to equation following:

$$\mathbf{A = -Log\ (\frac{I}{I_0}) = -Log\ T}$$

I_0 : represents the incident intensity.

I : represents the transmitted intensity.

T : represents the transmittance.

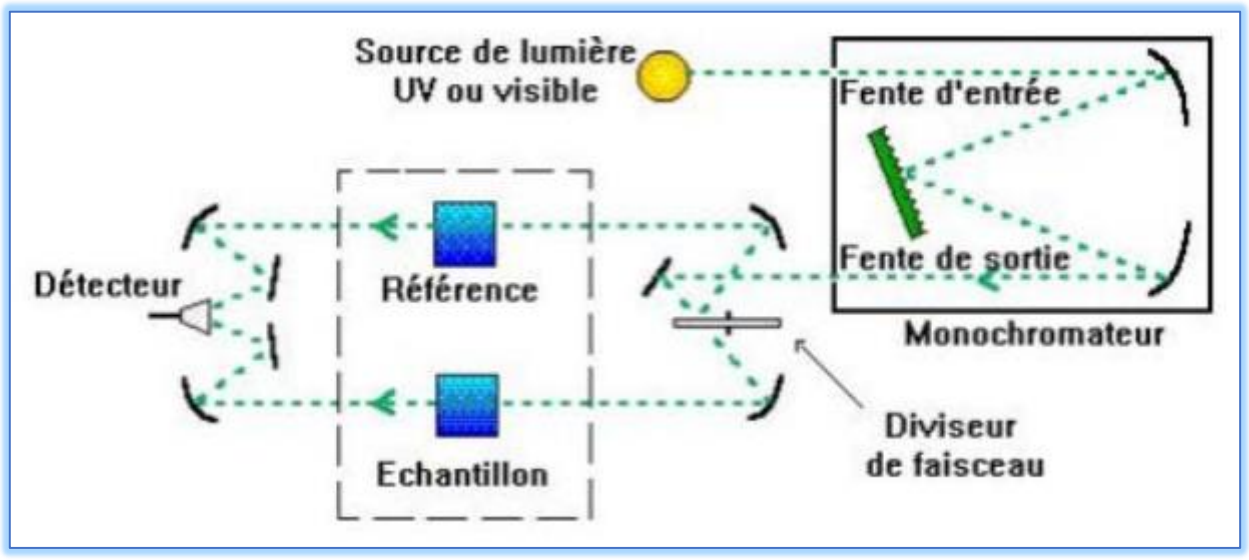

Figure II-5: Schema of the principle of the UV-Vis spectroscopy[75].

I-8- Conclusion:

Iron oxide nanoparticles (IONPs) have become indispensable in various applications due to their unique properties and versatility. In the field of catalysis, IONPs serve as efficient catalysts for a wide range of reactions, including biodiesel production and environmental remediation. Their high surface area and unique surface chemistry enable them to catalyze reactions with high efficiency and selectivity, making them valuable in enhancing reaction rates and product yields. Additionally, IONPs are extensively used in environmental applications, particularly in water treatment processes. Their magnetic properties allow for easy separation from aqueous solutions, making them effective adsorbents for removing pollutants and contaminants from water, thus contributing to the preservation of clean water resources.

CHAPTER II: FOOD SECURITY AND DETECTING ASCORBIC ACID

II-1- Introduction:

Ensuring food security involves controlling spoilage compounds to maintain the safety, quality, and nutritional value of food products. Spoilage compounds, such as microbial toxins, off-flavors, and undesirable metabolic byproducts, pose significant risks to food safety and can lead to considerable economic losses. Effective control strategies encompass stringent hygiene practices throughout the food production and supply chain, the use of preservatives and natural antimicrobials, and the adoption of advanced packaging technologies like modified atmosphere packaging (MAP) and vacuum sealing. Additionally, regulating storage conditions—such as temperature, humidity, and light exposure is crucial for inhibiting the growth of spoilage organisms and slowing chemical degradation[76, 77].

Detecting spoilage compounds is essential for ensuring food safety, quality, and shelf life. These compounds, such as microbial toxins and off-flavors, can compromise food products and pose health risks. Early detection allows for timely intervention, preventing the distribution of spoiled food and protecting public health. It also helps maintain hygiene standards and reduces economic losses from food waste. Advanced detection methods, including chemical assays and biosensors, provide rapid and reliable results, ensuring that consumers receive safe and high-quality food, thereby reinforcing food security and consumer trust[78-79].

II-2- Definitions of Food Security:

Food security is a flexible concept as reflected by the many attempts to define it in research and policy usage. The concept of food security originated some 50 years ago, at a time of global food crises in the early 1970s. Even two decades ago, there were about 200 definitions for food security in published writings (Maxwell and Smith, 1992), showing the contextual dependent features of the definition. The current widely accepted definition of food security came from the Food and Agriculture Organization (FAO) annual report on food security “The State of Food Insecurity in the World 2001”: Food security is a situation that exists when all people, at all times, have physical, social and economic access to sufficient, safe and nutritious food that meets their dietary needs and food preferences for an active and healthy life (FAO, 2002). The last revision to this definition happened at the 2009 World Summit on Food Security which added a fourth dimension – stability – as the short-term time indicator of the ability of food systems to withstand shocks, whether natural or man-made (FAO, 2009)[80-82].

II-3- Control of food security:

The control of food security is essentially based on controlling spoilage compounds in the food. The term "**spoilage compounds**" typically refers to substances produced during the degradation of food, leading to undesirable changes in flavor, odor, texture, or appearance[83]. For example:

- **Change in color:** the fruits like banana turn black after storing for a long time and reduce the acceptability of the food.
- **Change in smell:** rancid smell of spoil ed oils, fatty food, bitter smell of curd or sour smell of starchy food. (Rancid samosa, potatoes wada, chakli, etc.)
- **Change in consistency:** curdling of milk, stickiness and undesirable viscosity in the spoiled cooked legumes, curries and vegetables.
- **Change in texture:** some vegetables like potatoes, brinjal, carrots etc. undergoes too much softening leading to rotating, change in firmness. Lump formations take place in powdered material (milk powder, wheat flour).
- **Changes due to mechanical damage:** mechanical damage such as eggs with broken shells, bruising of the fruit and vegetables during harvesting, packaging, transportation and handling causes damage[84, 85].

These changes are often caused by microbial activity, chemical reactions, or enzymatic processes.

Spoilage compounds are more often associated with microbial growth and the production of substances like:

- **Amines** (e.g., histamine in fish).
- **Organic acids** (e.g., lactic acid in dairy products).
- **Sulfur compounds** (e.g., hydrogen sulfide in spoiled eggs)[86, 87].

II-4- Definition of vitamins:

Vitamins are essential nutrients required by the body in small amounts for various physiological functions. While some vitamins can degrade over time or under certain conditions (such as exposure to light, heat, or air), leading to a loss of nutritional value, vitamins such as ascorbic acid and thiamine are considered as a spoilage compounds[88, 89]. For example:

II-4-1- Vitamin C:

Ascorbic acid can degrade and lose its potency when exposed to air and light, but its degradation products are not typically considered spoilage compounds[90].

II-4-2- Vitamin B1:

Thiamine can be lost during cooking or storage, but this loss does not usually result in spoilage[91].

II-5- Definition of food spoilage:

Food spoilage is a contamination condition that occurs as a result of the growth and reproduction of harmful microorganisms such as bacteria, fungi, viruses, and parasites in food. These rots can cause food to spoil and become unfit for human consumption, causing foodborne illnesses that can range from mild digestive disorders to serious, life-threatening conditions. Food spoilage is caused by several factors, including poor storage, inappropriate temperatures, contamination of foods during preparation or transportation, and failure to follow good hygiene practices[86, 92].

II-6- Methods used in preventing food spoilage:

There are several methods that are used in preventing food from spoilage. Researchers are totally focused on techniques and methods to prevent the spoilage of that food products which are used in everyday life[93].

II-6-1- Physical Methods:

There are many physical methods used such as canning, drying and fermentation to control food spoilage. The growth and reproduction of microbes is affected by temperature, radiation, water activity[94].

II-6-2- Chemical Methods:

Chemical method has been classifying chemical incorporation into the food preservation and additive's purpose. In traditional method of preservation some household substances like sugar, salt, and spices, wood-smoke are used[95].

II-6-3- Microbial spoilage:

Microbial spoilage is caused by microorganisms like fungi (molds, yeasts) and bacteria. They spoil food by growing in it and producing substances that change the color, texture and odor of the food. Eventually the food will be unfit for human consumption[96].

II-6-4- Bioactive food packaging:

It is a new technique is used for the prevention of food from food-spoilage microorganisms. For this used active extracts from agro-industrial sub products (Almond shells, and grape pomace) with antioxidant activity that developed for antimicrobial benefits to bioactive packaging. It is used against food pathogenic bacteria like E. coli, and Salmonella[97, 98].

II-7- Vitamins C or ascorbic acid:

Vitamins are found in a variety of foods such as fruits, vegetables, meat, fish, nuts and seeds. Some vitamins can also be manufactured within the body through exposure to sunlight, such as vitamin D[99].

II-7-1- Definition of vitamin C:

Vitamin C, also known as ascorbic acid, is a water-soluble vitamin that cannot be synthesized by the human body, so it must be obtained through the diet. Vitamin C plays a vital role in many biological functions, including boosting the immune system, acting as an antioxidant, and supporting overall health by promoting collagen formation and iron absorption.[90]

II-7-2- Vital roles and functions of vitamin C:

- **Anti-oxidant**: vitamin C helps protect cells from damage caused by free radicals, which may contribute to the development of chronic diseases such as heart disease and cancer.
- **Collagen formation**: it is necessary for the formation of collagen, the primary protein in connective tissues such as skin, blood vessels, tendons, and ligaments.
- **Iron absorption**: promotes the absorption of non-heme iron (iron found in plants), which helps prevent iron deficiency anemia.

- **Boost the immune system**: it plays a role in enhancing immune system function by stimulating white cell production and strengthening skin barriers.
- **wound healing** : it contributes to accelerating the wound healing process through its role in collagen formation **[90, 100]**.

II-7-3- Food sources of vitamin C and recommended quantities:

- **Fruits**: orange, lemon, kiwi, strawberry, guava.
- **Vegetables**: red and green peppers, broccoli, spinach, sweet potatoes.
- **Other sources**: fortified fruit juices, nutritional supplements.

According to the National Institutes of Health (NIH), recommended amounts of vitamin C vary by age and gender, as follows:

- Adult men: 90 mg/day.
- Adult women: 75 mg/day.
- Pregnant women: 85 mg/day.
- Breastfeeding women: 120 mg/day.

Vitamin C is considered safe when taken within recommended amounts. However, high doses (more than 2,000 mg/day) can cause side effects such as: diarrhea. Nausea. Abdominal cramps.**[101]**

Vitamin C deficiency: Vitamin C deficiency can lead to scurvy, a rare but serious condition characterized by the following symptoms**[102]**:

- Fatigue and general weakness.
- Gingivitis and bleeding.
- Joint and muscle pain.
- Poor wound healing.

II-8- Oxidized ascorbic acid/ Ascorbate biosensors:

II-8-1- Definition of biosensors:

Biosensors are devices that convert a biological response into an electrical signal. Biosensors must be very specific, independent of physical conditions such as pH and temperature, and reusable. Cammann coined the word "**biosensor**," and the IUPAC standardized it. Multidisciplinary research

in chemistry, biology, and engineering is required to fabricate biosensors, their materials, transducing devices, and immobilization procedures (Fig. II-1).

Biosensor is a low cost; simple apparatus (or no instrumentation in the case of naked-eye detection); the ability to be qualitatively or semi qualitatively detected by the naked eye. Being water soluble vitamin in nature, ascorbic acid does not attain very high level in biological fluids[103].

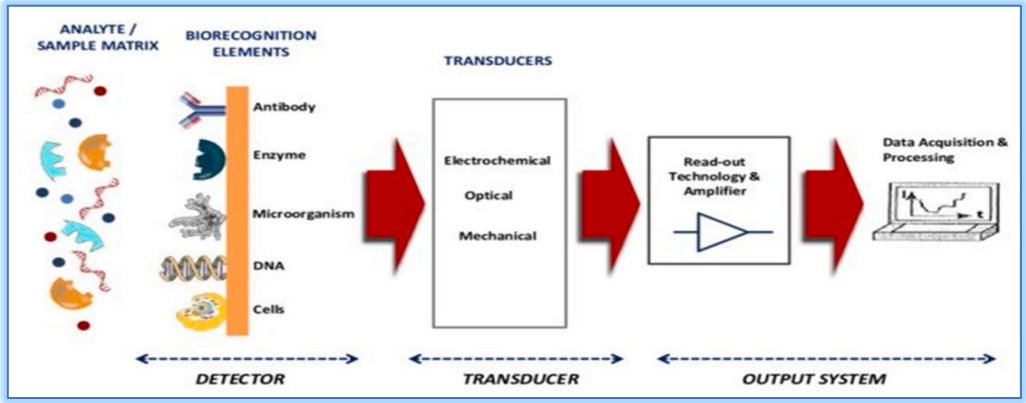

Figure II.1: Schematic representation of biosensor principle[103].

Several ascorbate biosensors are use in order to detecting vitamin C such as electrochemical biosensor and colorimetric detection essay.

II-8-2- Electrochemical ascorbate biosensor:

The electrochemical biosensor is one of the typical sensing devices based on transducing the biochemical events to electrical signals. In this type of sensor, an electrode is a key component that is employed as a solid support for immobilization of biomolecules and electron movement. This biosensor is a potential for making low-cost, easy-to-use portable devices for various uses, including medical diagnostics and environmental monitoring; Nanomaterials such as carbon nanotubes and graphene have resulted in new improvements in electrochemical sensors and future directions for the discipline[104].

II-8-3- Colorimetric ascorbate biosensor:

The colorimeter biosensor's operating principle is based on Beer Lambert's law, which states that the amount of light absorbed by a color solution is directly proportional to its concentration, the length of a light path through it and wavelength dependent molar absorptivity coefficient. The

colorimetric probe 3,3′,5,5′, tetramethylbenzidine (TMB) was used to develop a ’turn–off’ technique for the detection of ascorbic acid **[105, 106]**Figure II.2.

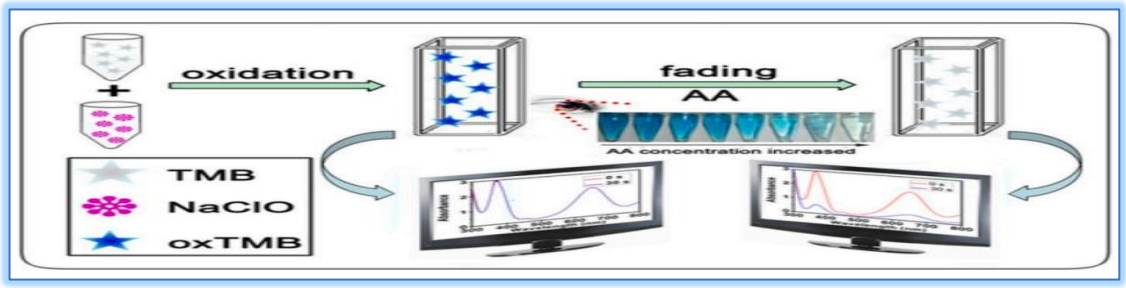

Figure II.2: Schematic illustration of colorimetric platform for sensing ascorbic[102].

blue color and a drop in absorbance at 652 nm. Within the dynamic working range of 1–70 µM with a detection limit of 0.58 µM, an excellent linear relationship between absorbance and ascorbic acid concentration was achieved under ideal conditions. Furthermore, with an average relative error of 3.3%, the acquired results were like those measured by high-performance liquid chromatography[102].

II-8-3-1- Ascorbate detection by aggregation of gold nanoparticles (AuNPs) in the presence of chromium (Cr)

The principle of ascorbate detection by aggregation of gold nanoparticles (AuNPs) in the presence of chromium (Cr) involves a different step[105]:

II-8-3-1-1- Reduction of Chromium (VI) to Chromium (III):

Ascorbic acid (ascorbate, AA) can reduce toxic chromium (VI) (Cr (VI)) to the less toxic chromium (III) (Cr (III)). The reaction between ascorbic acid and Cr (VI) results in the oxidation of ascorbic acid to dehydroascorbic acid[105, 106].

II-8-3-1-2- Interaction with Gold Nanoparticles:

Gold nanoparticles are typically stabilized and remain in a dispersed state in a colloidal solution. The interaction between Cr (III) and gold nanoparticles can lead to the aggregation of AuNPs [106-108].

II-8-3-1-3- Colorimetric Change and detection:

When gold nanoparticles aggregate, there is a shift in the surface plasmon resonance (SPR) band, leading to a visible color change in the solution. Dispersed AuNPs typically exhibit a red color due to their SPR peak around 520 nm. Upon aggregation, this peak shifts to a longer wavelength, and the solution changes color, often to blue or purple. The degree of aggregation, and thus the color change, can be correlated with the concentration of ascorbic acid present. By measuring the absorbance at specific wavelengths using a UV-Vis spectrophotometer, the concentration of ascorbic acid can be quantified[106, 107].

II-8-3-1-4- Aggregation of AuNPs:

Cr (III) interacts with the gold nanoparticles, causing them to aggregate. This aggregation disrupts the stabilization of the nanoparticles and leads to a change in their optical properties[107].

II-8-3-1-5- Colorimetric Change:

The shift in the SPR band due to aggregation causes a visible color change from red to blue or purple, which can be measured[107, 108].

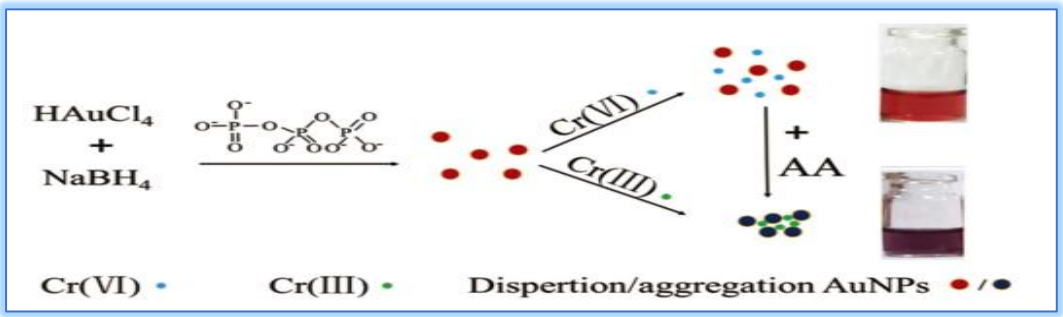

Figure II.3: Colorimetric detection based on Au nanoparticle's aggregation[108].

II-8-3-2-Ascorbate detection by using molybdenum (Mo) and iron oxide nanoparticles

Colorimetric detection of ascorbic acid (ascorbate) using molybdenum (Mo) and iron oxide nanoparticles involves a series of chemical reactions and interactions that result in a color change

(from colorless to blue), which can be measured spectrophotometrically. This essay involves different steps[106]:

- **Reduction Reaction:**

Ascorbic acid acts as a reducing agent. When ascorbic acid is present, it reduces the molybdenum (VI) to a lower oxidation state, such as molybdenum(V) or molybdenum (IV).

- **Interaction with Iron Oxide Nanoparticles:**

The reduced molybdenum species interact with iron oxide nanoparticles. These interactions can cause changes in the optical properties of the iron oxide nanoparticles, leading to a visible color change.

- **Colorimetric Detection:**

The resulting color change can be quantified by measuring the absorbance at specific wavelengths (**820 nm**) using a UV-Vis spectrophotometer. The intensity of the color is proportional to the concentration of ascorbic acid present in the sample.

II-9- Conclusion:

In conclusion, food security is crucial as it ensures an adequate, safe, and nutritious food supply for everyone. This importance is highlighted by the risks of food spoilage, which pose major health threats due to contamination by harmful microorganisms. Preventing these risks requires strict hygienic practices throughout food production, storage, and preparation. Additionally, essential vitamins are vital for overall health and a strong immune system, emphasizing the need for a balanced and varied diet to provide all necessary nutrients. Thus, achieving food security is a complex challenge that demands coordinated efforts to ensure the availability of safe and healthy food, with a focus on preventing spoilage and meeting basic nutritional needs for all.

CHAPTER III: STUDY OF COLORIMETRIC DETECTION OF AA BY BIOSENSORS MO (VI)/IONPs

III-1- Introduction

This study investigates the colorimetric detection of ascorbic acid (AA) by Mo (VI)/IONPs biosensors. This work aims to study the catalytic activity of four greenly synthesised IONPs as biosensors for the colorimetric detection of AA by using the phosphomolybdenum; Mo (VI) which reduces to Mo (V). This latter will be reduced from MO (VI) to MO (V) by AA. The effect of the pH of buffer solution (from 1 to 5) and interference of different interferents on the colorimetric detection of AA will be studied in detail. A series of aqueous solution of AA were prepared in the range of 0.5-200mM.

In this chapter, we will describe the methodology followed to carry out this study. In the first part, we will present the characterisation of used IONPs. In the second part, we will detail the, we studied the experiment to determine the extent of the effect of iron oxide particles on the interaction between molybdate and ascorbic acid. We prepared the following solutions: Preparation of Molybdate Reagent solution and Preparation of Aqueous Ascorbic acid solutions.

III-2- Green synthesis of iron oxides nanoparticles

III-2-1- Chemicals and Apparatus

➢ Chemicals:

The plant used in this study are*: Artemisia herba-alba. (L) (Asteraceae family)*, *Matricaria Pubescens (L) (Asteraceae family)*, *Juniperus Phoenicia. (L) (Cupressaceae family)*, *Rosemarinus officinalis. (L) (Lamiaceae family)*, iron chloride ($FeCl_3$, $6H_2O$ (99%), Biochem chemopharma), and bi-distilled water.

➢ Apparatus:

The table summarizes the apparatuses used in this study.

Table III-1: Apparatus used to characterisation of IONPs.

Apparatus	Purpose
UV-Visible spectrophotometer M300	Characterisation of IONPs
FTIR spectrophotometer (Nicolet iS5, Thermo Fisher Scientific)	Characterisation of IONPs
XRD ((RigakuMiniflex 600) with (30 keV, 30 mA) as conditions of X-ray generation and Kα radiation of copper λ = 1:54056 A)	Determine the crystal structure of iron oxide particles
SEM (FEI Quanta 250 with a tungsten filament)	Study the surface composition and determine the morphological features such as size, shape, and surface distribution of particles

III-2-2- Preparation of plant extracts

For the separation of natural materials from the raw material with the use of solvents, if the material that we want to separate is solid in this case we apply solid-liquid extraction. The principle of this method is that the solvent must cross the solid-liquid interface barrier, dissolve the active component inside the solid and carry it out. In our study, for the extraction of phenolic compounds using the maceration extraction technique[109].

In the first step, the plants were thoroughly washed with distilled water. After drying, they were ground into a fine powder. 30 grams of each plant powder were mixed with 540 mL of distilled water. The mixtures were stirred continuously for 24 hours using a motor at ambient temperature. Finally, the extracts were passed through two layers of gauze, followed by filtration through 0.22 µm Millipore filters. The resulting filtrates were used in subsequent nanoparticle synthesis reactions.

III-2-3- Green synthesis of iron oxide nanoparticles

For the green synthesis of iron oxide NPs, we followed the protocol as follows[109, 110]: 200 ml of plant aqueous extract is mixed with 100 ml of aqueous iron chloride salt solution with a concentration of 0.4 M. The mixtures are stirred continually for 1h at reaction temperature 70 °C. They are then dried in the drying oven. stirring and heating 70 °C (Figure III.1).

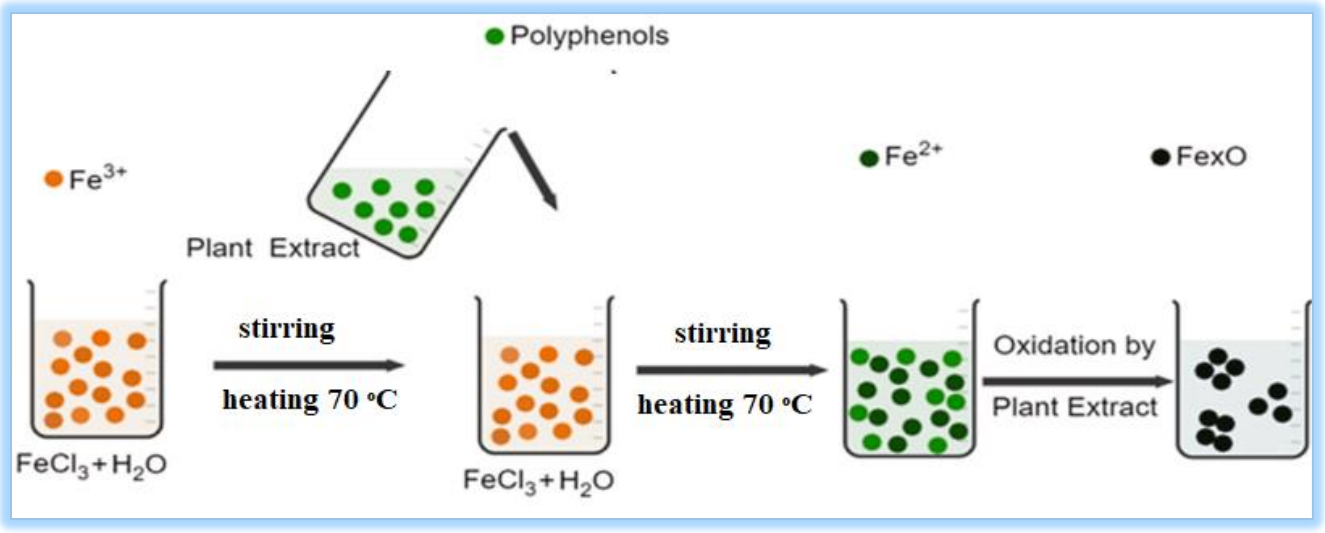

Figure III.1: Protocol used in the green synthesis of iron oxide nanoparticle.

III-3- Results and discussion

III-3-1- Characterization of Four Magnetite NPs

The eco-friendly synthesis method of freshly prepared iron oxides NPs as well as their characterization are thoroughly detailed in our previous work[109, 110]. In the eco-friendly synthesis of iron oxide NPs, the bioactive compounds in mediating plant extract including polyphenols play a crucial role as a reducing agent. The overall reaction mechanism involving the reduction of iron ions and the formation of iron oxide NPs can be described as follows:

1- Ferric ions (Fe^{+3}) are reduced to ferrous ions (Fe^{+2}) by the bioactive compounds in the plant extract as presented in the next equation:

$$2Fe^{+3} + \text{Polyphenols} \longrightarrow 3Fe^{+2} + \text{Oxidized product}$$

2- Nucleation and formation of Iron (II) Oxide NPs (FeO) as presented in the next equations:

$$nF\ e^{+2} \longrightarrow \text{Nuclei}$$

$$\text{Nuclei} + \frac{1}{2}O_2 \longrightarrow FeO$$

3- In the presence of oxygen, the formed FeO NPs can undergo oxidation to produce Fe_3O_4 NPs as presented in the next equation:

$$6FeO + O_2 \longrightarrow 2Fe_3O_4$$

Chen et al reported that after four months of storage of FeO NPs under ambient conditions, FeO NPs are completely oxidized to form a single phase of Fe_3O_4 NPs. For this reason, after ending the synthesis, obtained iron oxide NPs (FeO NPs + Fe_3O_4 NPs) are stored for four months under the ambient conditions to obtain one single phase of NPs which is Fe_3O_4 NPs.

III-3-2- X-ray Diffraction Analysis of Four Magnetite NPs:

The XRD patterns of the four iron oxide NPs samples are presented in Figure III.2, and all exhibit Bragg reflection peaks at identical angles, however with different peak intensities. These differences are mainly due to mediating plant extract.

Figure III.2 shows that peaks appear at around 2θ° = 52.60°, 49.80°, 42.50°,41.40°, 41.00°, 37.10°, 32.30°, 30.80°, 29.95°, 25.60°, 22.52°, 20.30°, 16.70° and 16.20°. All of these peaks correspond to the Fe_3O_4 phase and are consistent with the Miller indices 644, 534, 522, 251, 250, 404, 106, 106, 400, 030, 212, 210 and 021 respectively, according to standard diffraction of orthorhombic Fe_3O_4 NPs as defined in the JCPDF file 01-076-0958 except for minor differences in intensities and a shift in 2θ° values arising from defects within magnetite NPs structures.

The average diameters of the magnetite NPs samples, presented in Table 2, were calculated using the next equation of Scherrer's:

$$D = \frac{0.9\lambda}{\beta\cos\theta}$$

Where θ, λ, and β represent the Bragg angle, the X-ray wavelength (1.54056 °A), and the full width at half-maximum (FWHM) of the most intense diffraction peak D represents the average diameter of the magnetite NPs. The most useful information to be extracted from XRD patterns, in additionally to the average diameters, is the lattice parameters of Fe_3O_4 NPs samples. For orthorhombic crystal cells, lattice parameters are calculated using the following equation:

$$\frac{1}{d_{hkl}^2} = \frac{h^2}{a^2} + \frac{k^2}{b^2} + \frac{l^2}{c^2}$$

Where, d_{hkl}, (hkl), and (a, b, c) are the inter-planer distance, Miller indices, and lattice parameters respectively. For Fe_3O_4 orthorhombic crystal cells, standard d_{hkl} = 2.96700°A, and standard lattice parameters are a = 11.8680°A, b = 11.8510°A, and c = 16.7520°A. The lattice parameters of the four orthorhombic magnetite NPs samples are calculated in the most intense diffraction peaks. a (°A) is

calculated with the help of peak 400, b (˚A) is calculated with the help of peak 030, and c (˚A) is calculated with the help of peak 021.

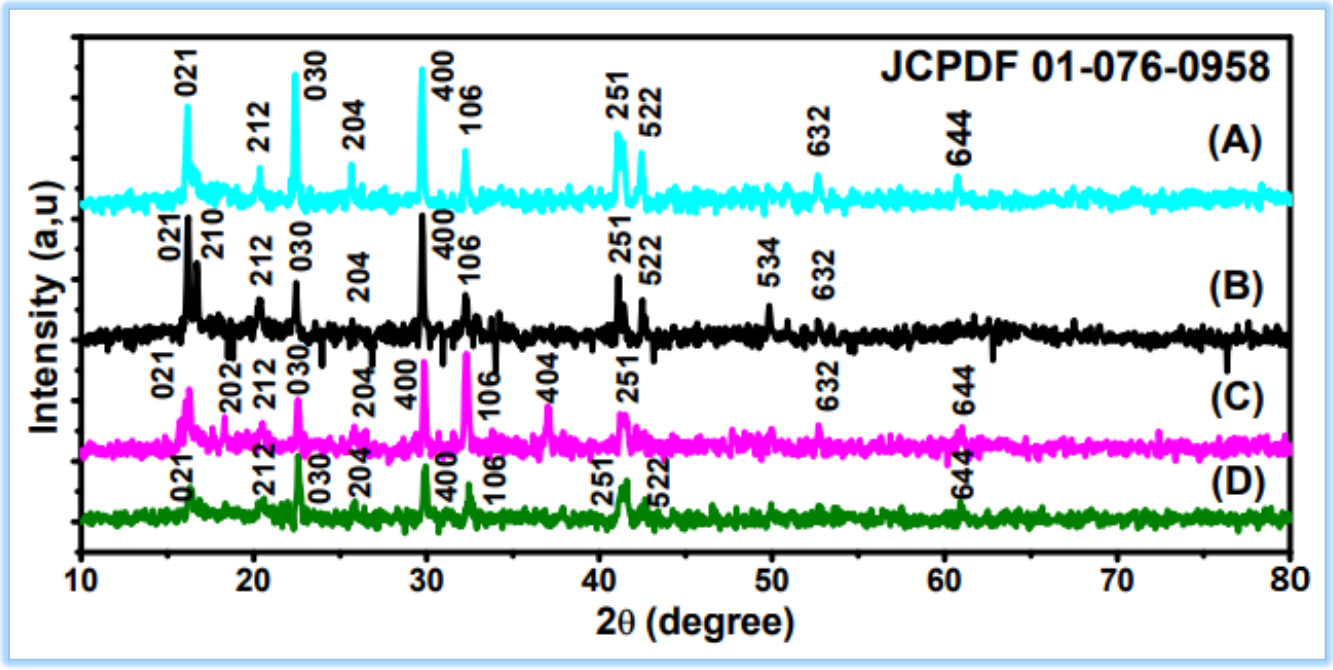

Figure III.2: XRD patterns of four magnetite NPs (A) ROS−Fe_3O_4, (B) ARM−Fe_3O_4, (C) MAT−Fe_3O_4 and (D) JUN−Fe_3O_4, JCPDF file 01-076-0958.

Table III.2: Crystallographic data obtained from XRD patterns of four magnetite NPs.

Magnetite NPs	Average Diameter (nm)	Calculated d (˚A)	Lattice parameters (˚A)		
ARM−Fe_3O_4	41.49	2.97336	a = 11.8934	, b = 11.84151	c = 14.4107
ROS−Fe_3O_4	39.89	2.97395	a = 11.8958	b = 11.83656	c = 14.4466
MAT−Fe_3O_4	33.13	2.97525	a = 11.9010	b = 11.82426	c = 14.5370
JUN−Fe_3O_4	29.27	2.97109	a = 11.8844	b = 11.81994	c = 14.5690

When comparing the calculated lattice parameters presented in Table III-2 with the lattice parameters of the cell, minor differences are remarked due to defects within magnetite NPs structures.

Furthermore, the results showed that the particle sizes of the magnetite samples vary with the variation of the plant extract used in their eco-friendly synthesis. The average diameter of the ARM−Fe_3O_4, ROS−Fe_3O_4, MAT−Fe_3O_4, and JUN −Fe_3O_4 NPs, presented in Table III-2, are, respectively, 41.49, 39.89, 33.13, and 29.27nm.

It is well-known that the bioactive compounds including polyphenols and organic acids in the plant extract, play a crucial role in stabilizing the formed iron oxide nanoparticles (NPs). These compounds attach to the nanoparticle surfaces, preventing agglomeration and ensuring stability, thereby reducing the diameter of the particles. Mediating extracts' acidic pH of ARM−Fe_3O_4, ROS − Fe_3O_4, MAT−Fe_3O_4, and JUN−Fe_3O_4 NPs were, respectively, 5.25, 5.05, 4.63, and 3.69. Consequently, the average diameter of Fe_3O_4 NPs samples decreases with the increasing acidity of the plant extract. This finding aligns with the results reported by Makarov et al. In their study, the authors environmentally prepared two samples of Fe_3O_4 NPs using H. vulgare plant extract with a pH of 5.8 and R. acetosa plant extract with a pH of 3.7. They observed that Fe_3O_4 NPs prepared using a less acidic plant extract exhibited smaller diameters.

III-3-3 FT-IR Spectroscopic Analysis of Magnetite NPs:

FTIR spectroscopy is commonly used as an identification technique to obtain an idea about the phase of iron oxide NPs. Each iron oxide phase produces a distinguishable IR spectrum. The FTIR spectra of the four iron oxide NPs, which were recorded between 4000 and 500 cm^{-1}, are shown in Figure III.3.

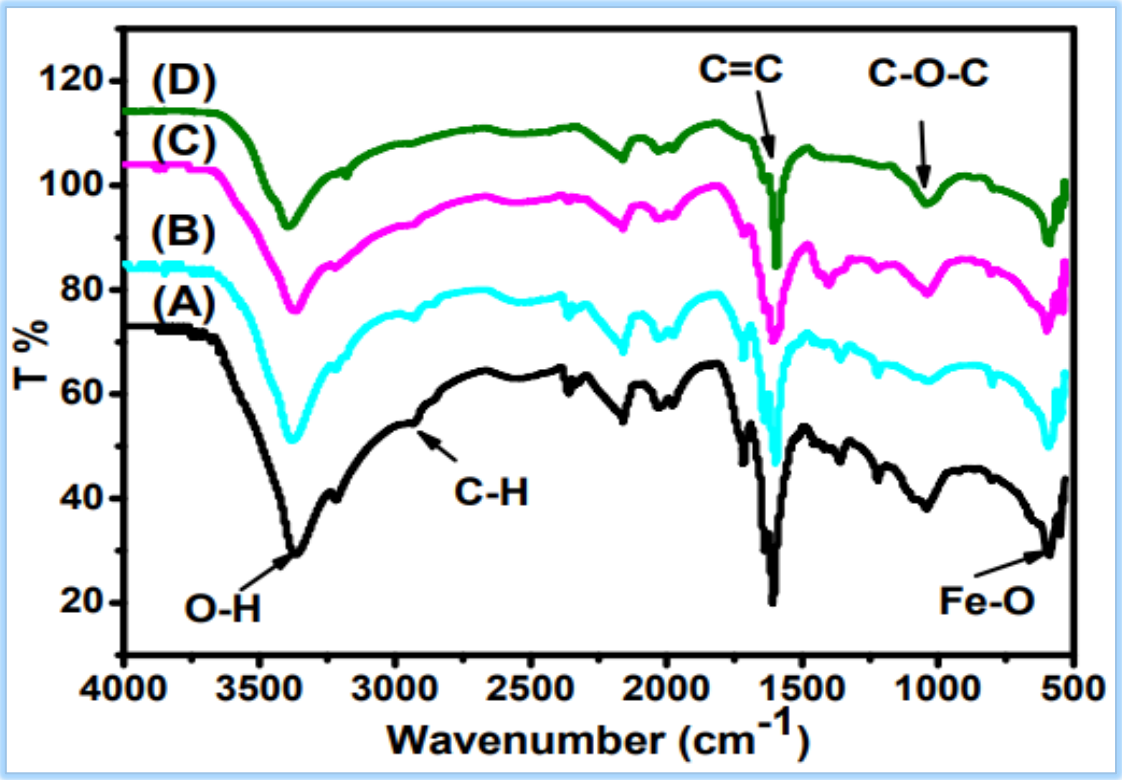

Figure III.3: FTIR spectra of eco-friendly prepared of (A) ARM−Fe_3O_4, (B) ROS−Fe_3O_4, (C) MAT−Fe_3O_4, and (D) JUN−Fe_3O_4 NPs.

Table III.3: FTIR Spectra of four magnetite NPs Show varied vibration ranges of functional groups.

Sample	O−H (cm^{-1})	C−H (cm^{-1})	C=C (cm^{-1})	C−O−C (cm^{-1})	F e−O (cm^{-1})
ARM−Fe_3O_4	3267	2932	1590	1036	593
ROS−Fe_3O_4	3250	2930	1591	1039	592
MAT−Fe_3O_4	3236	2930	1591	1040	592
JUN−F e_3O_4	3223	2929	1595	1039	594

Table III-3 summarizes the different peak ranges observed in the IR spectra of the four nanoparticle samples (Figure 4(A), (B), (C), and (D)). Peaks at 3223−3267cm^{-1} are attributed to O−H stretching vibration, while peaks at 2930−2932cm^{-1} correspond to C−H aromatic and C−H aliphatic vibrations of Fe_3O_4 NPs. Peaks at 1590−1595cm^{-1} correspond to C=C stretch in aromatic rings and anti-symmetric stretching of the carboxylate groups (COO^-), whereas peaks at 1033−1045cm^{-1} are assigned to the C−O−C of the phenolic groups. Additionally, the peak observed at around 590 cm^{-1} is attributed to the Fe−O stretching band of Fe_3O_4 NPs.

III-3-4- UV-Vis Spectroscopic Analysis of Four Magnetite NPs:

To determine the band gap energies of the four Fe_3O_4 samples, their optical absorbance spectra were measured within the wavelength range of 200−900 nm. The band gap (Eg) and the linear optical absorption coefficient (α) of a band gap semiconductor are connected through the following equation:

$$\alpha h\nu = A(h\nu - Eg)^n$$

In Eq, hν represents the energy of a photon, A is a constant of proportionality, and the value of the exponent n depends on the type of electronic transition that occurs for indirectly allowed transitions n = 2, while for direct allowed transitions n = 1/2.

The band gap energies of the four magnetite samples were determined using the extrapolation of the linear portion of the plot $(\alpha h\nu)^2$ vs αhν (Figure) for direct transition Eg values, and the plot $(\alpha h\nu)^{1/2}$ vs αhν (Figure III-4) for indirect transition Eg values.

The estimated direct and indirect band gap energies of the four magnetite samples are presented in Table III-4. The direct band gap energy Eg values for ARM−Fe_3O_4, ROS−Fe_3O_4, MAT−Fe_3O_4 and JUN−Fe_3O_4 NPs are 2.87eV, 2.95eV, 2.96eV and 2.97eV respectively. These values are comparable to the result obtained by Kamakshi et al. Where they reported a direct band gap energy of 2.76 eV for magnetite NPs. Indirect band gap energy values were also estimated for the four samples using the same method and are also shown in Table 4. The estimated indirect Eg values for ARM−Fe_3O_4, ROS−Fe_3O_4, MAT−Fe_3O_4, and JUN−Fe_3O_4 samples were found to be 2.51, 2.55, 2.60 and 2.64eV respectively, which are comparable to the indirect Eg reported in reference (Eg = 2.53eV).

The estimated direct and indirect band gap energies of the four magnetite samples fall within the range of band gap energies of semiconductors, which typically range from 0-3 eV. Therefore, it is reasonable to classify the four magnetite samples as semiconductors based on their band gap energies.

Furthermore, it is found that the diameter of ARM−Fe_3O_4, ROS−Fe_3O_4, MAT−Fe_3O_4, and JUN−Fe_3O_4 NPs is respectively, 41.49, 39.89, 33.13 and 29.27nm. the smaller crystallite size of eco-friendly prepared Fe_3O_4 NPs is related to the higher direct and indirect Eg values as proof of the quantum size effect. So, the decrease in particle diameter leads to an increase in the Eg. This result is in agreement with that reported by Singh et al.

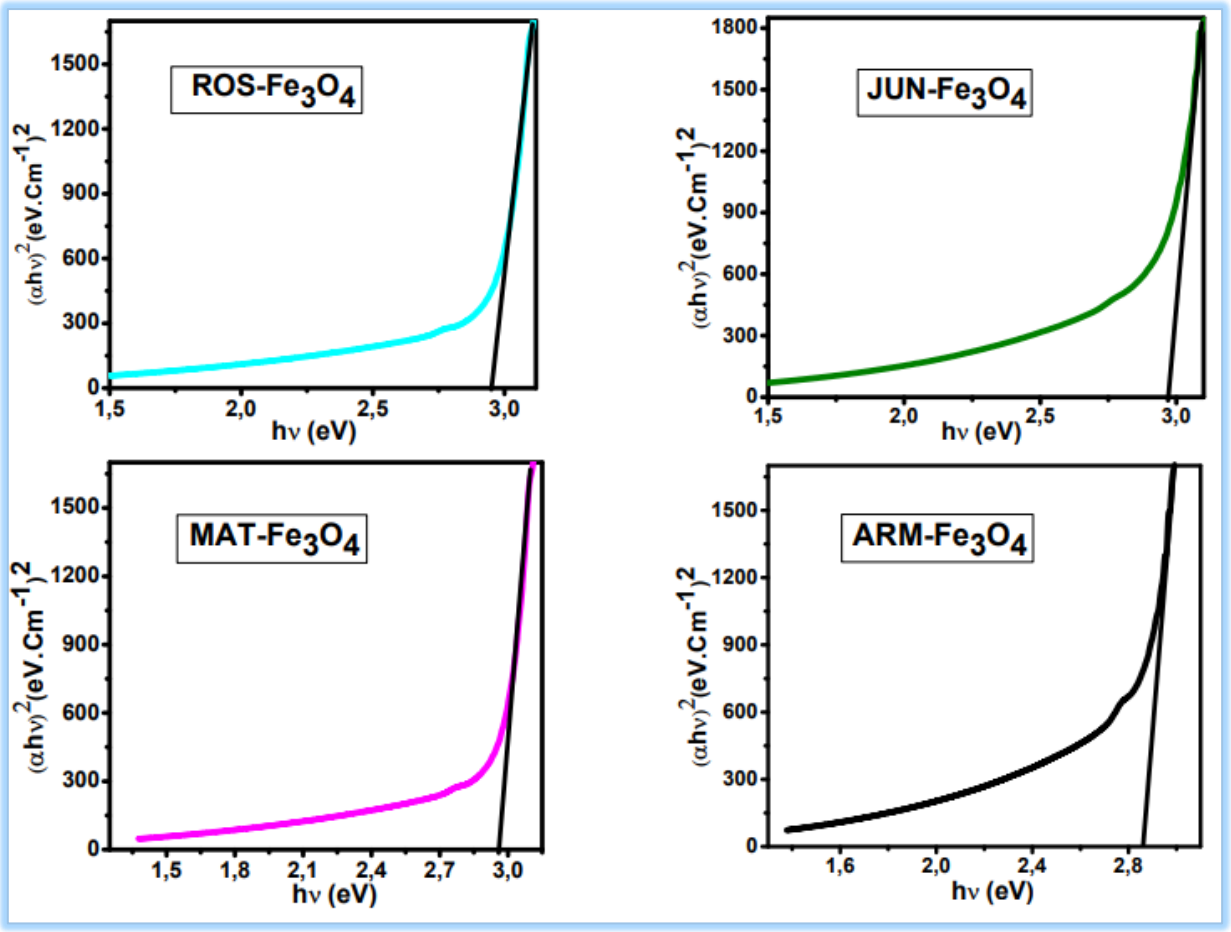

Figure III.4: Plots of $(\alpha h\nu)^2$ versus $(\alpha h\nu)$ for direct transition of four Fe_3O_4 samples sonicated in acetone for 15 minutes.

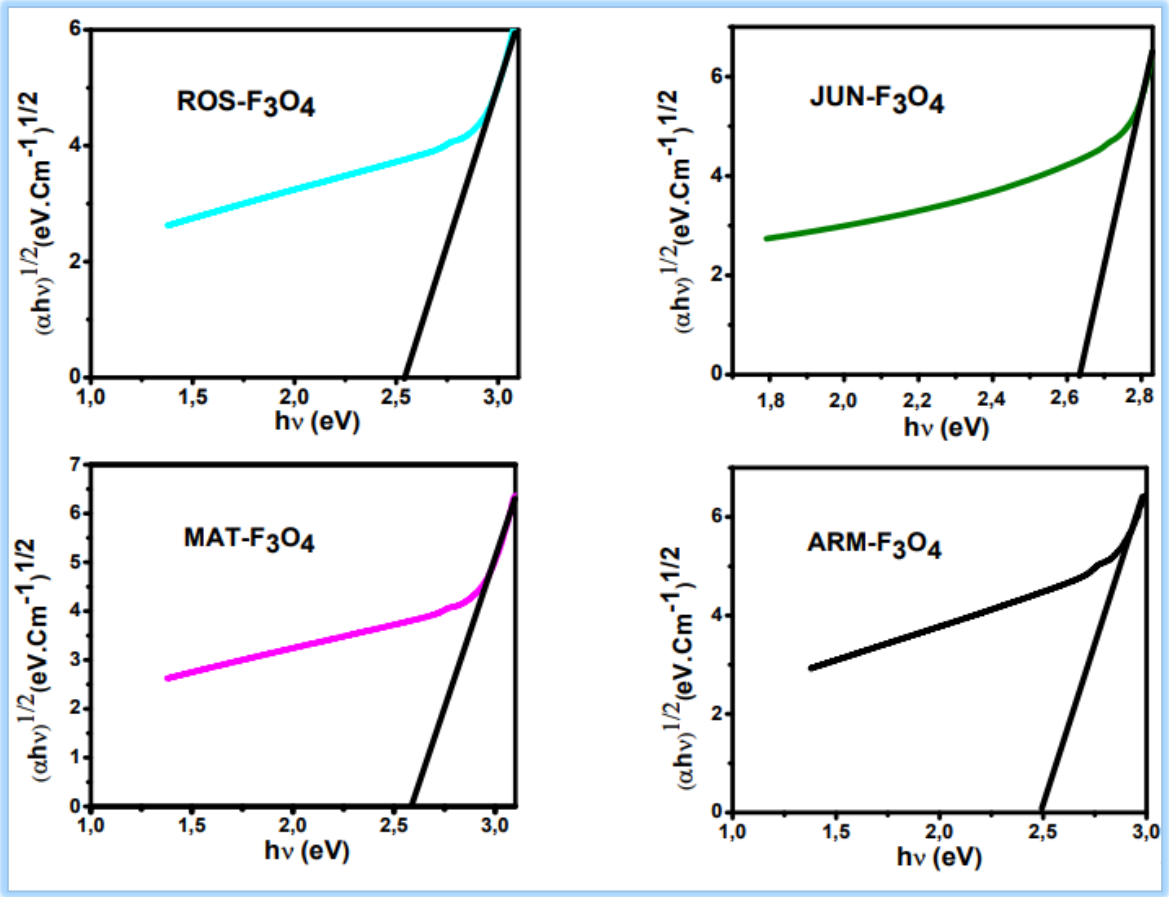

Figure III.5: Plots of $(\alpha h\nu)^{1/2}$ vs $(\alpha h\nu)$ for indirect transition of four Fe_3O_4 NPs sonicated for 15 minutes in acetone.

III-3-5- SEM Images of Eco-friendly Synthesised Magnetite NPs:

Figure III-5 depicts SEM images of the four magnetite samples synthesized using plant extract, revealing their irregular rock-like forms. Agglomerations resembling rocks are evident in the SEM image of JUN−Fe_3O_4 NPs (Figure III-5), while MAT−Fe_3O_4 NPs exhibit mountain-like structures with giant rocks (Figure III-5). ROS−Fe_3O_4 and ARM−Fe_3O_4 SEM images display occasionally big structured single bipyramids crystals, as observed in Figure III-5.

Table III.4: Estimated direct and indirect band gap energies of four magnetite NPs.

Sample	Direct Eg (eV)	Indirect Eg (eV)
ARM−Fe_3O_4	2.87	2.51
ROS−Fe_3O_4	2.95	2.55
MAT−Fe_3O_4	2.96	2.60
JUN−Fe_3O_4	2.97	2.64

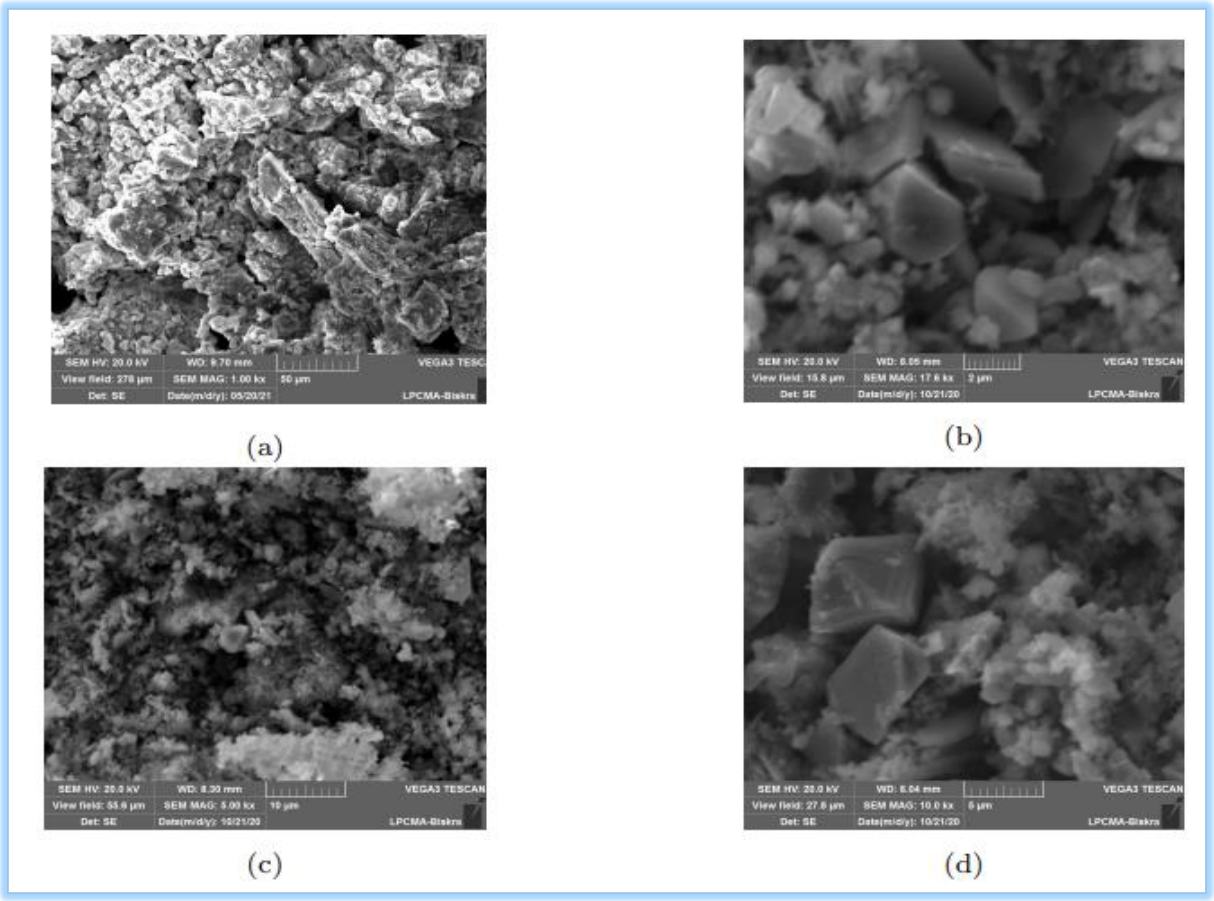

Figure III.6: SEM images of eco-friendly synthesised (a) JUN−Fe_3O_4, (b) MAT−Fe_3O_4 (c) ROS−Fe_3O_4, and (d) ARM−Fe_3O_4 samples.

III-4- Study of colorimetric detection of Ascorbic acid by four Mo (VI)/IONPs biosensors:

Among the most accessible methods, the colorimetric ones are particularly convenient and readily available in the laboratory. In this context, the direct spectrophotometric detection of ascorbic acid in this study:

III-4-1- Chemicals and Apparatus:

➢ Chemicals:

The chemicals used are listed in the table below:

Table III.5: Chemicals used in colorimetric detection of Ascorbic acid by Mo (VI)/IONPs

Chemical	Chemical Formula	Brand
Ammonium molybdate	Mo_7O_{24} (98%)	SIGMA ALDRICH
Phosphate sodium	NaH_2PO_4 (98%)	SIGMA ALDRICH
Sulfuric acid	H_2SO_4 (99.9%)	Biochem Chemopharma
Acetic acid	CH_3COOH (99%)	SIGMA ALDRICH
Vitamin C (Ascorbic Acid)	$C_6H_8O_6$ (99.8%)	Biochem Chemopharma
Sodium Acetate	$C_2H_3NaO_2$ (99%)	Biochem Chemopharma
hydrochloric acid	HCl (38)	Biochem Chemopharma
Hydroxyde sodium	NaOH (98%)	SIGMA ALDRICH
Calcium chloride	$CaCl_2$(95%)	SIGMA ALDRICH
Copper chloride	$CuCl_2$(99%)	SIGMA ALDRICH
Potassium chloride	KCl (95%)	SIGMA ALDRICH

III-4-2- Apparatus:

The details of the instruments used for sample preparation and spectroscopic measurements are mentioned in the table following:

Table III.6: Apparatus used in colorimetric detection of Ascorbic acid by Mo (VI)/IONPs biosensors

Apparatus	Purpose
UV-Visible spectrophotometer M300	Absorbance Measurement
pH metre (CONSORT C3010)	Measurement of the pH of buffer solution
Analytical Balance (Ohaus PX323)	Weight of samples
Ultrasound	Dispersing IONPs and distributing it throughout the solution

III-5- Experimental protocol used in the study of the colorimetric detection of AA by Mo (VI)/IONPs biosensors:

At the beginning of this experiment, we prepared the pH solution from 1 to 5, then we Preparation of Molybdate Reagent solution, then we Preparation of Aqueous Ascorbic acid solutions, then we diluted the mother solution into solutions of different concentrations from 0.5 to 200 mM.

III-5-1- Preparation of Molybdate Reagent solution:

To prepare 100 mL of reagent solution, dissolve 0.078g of Mo_7O_{24}, 0.33g of NaH_2PO_4, and 3.20 mL of concentrated H_2SO_4 in distilled water. Adjust the total volume to 100mL with distilled water (96.80mL).

III-5-2- Preparation of Aqueous Ascorbic acid solutions:

3.56g ascorbic acid in 100 mL distilled water, then was prepared various concentration of ascorbic 0.5 – 200 mM.

To make 0.5-200 mM dilutions (Figure**), we can use the equation below to calculate how much distilled water and 200mM AA solution we would need to add to make 5 mL of each of the target dilutions:

$$C_1 \cdot V_1 = C_2 \cdot V_2$$

Figure III-7: Preparation of different AA aqueous solution 0.5 – 200 mM.

III-5-3- Preparation of Buffer solutions (0.2 M) and the study of their effect on colorimetric detection of AA:

To prepare the buffer solution (BS), 2.7 g of sodium acetate and 0.6 mL of acetic acid are dissolved in 99.40 mL of distilled water. The pH of the solution is then adjusted using HCl and NaOH solutions to obtain pH values ranging from 1 to 5. The principle consists of introducing the electrode of a pH meter into a beaker containing the BS, previously adjusted. The determination of the pH is carried out by direct reading of the pH value. using a pH meter.

The colorimetric detection of AA was performed by the reduction of the Mo (VI) to Mo (V) in the presence of IONPs. Where, 2000 µl of Molybdate Reagent, 1200 µl of buffer solution (0.2M, pH=1-5) and 1200 µL different concentrations of AA (final concentrations: 0.5–200 mM) were mixed in a (5 mL tube). The absorbance variations at 820 nm were recorded by a UV-vis spectrometer after 1hour of the reaction at 95˚C. All followed steps are illustrated in next Figure.

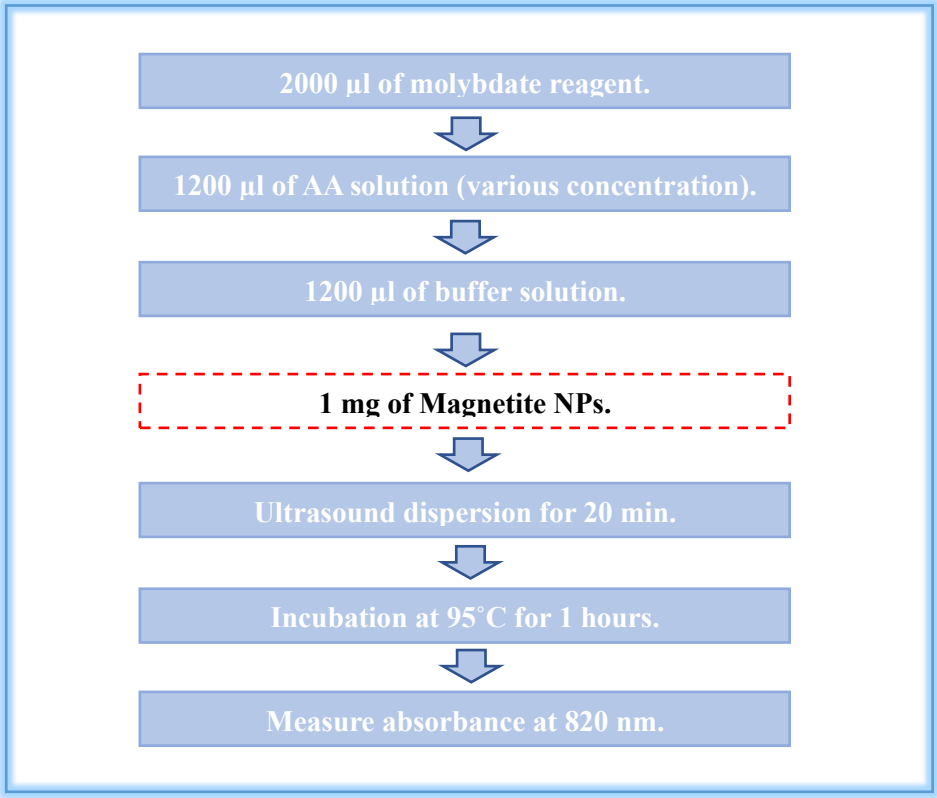

Figure III-8: protocol used in the study of buffer solution pH effect on the colorimetric detection of AA by Mo (VI)/IONPs biosensors**.**

III-5-4- Preparation of solutions of different interferents and their effect on the colorimetric detection of AA by Mo (VI)/IONPs biosensors:

To study the effect of different interferents on the oxidation reaction of AA with Mo (VI)/IONPs biosensors, we added masses of salts 0.11g (KCl), 0.13g ($CuCl_2$) and 0.075g ($CaCl_2$) to the AA aqueous solutions.

III-6- Results and discussion:

III-6-1- Study of the effect of the pH of buffer solution on colorimetric detection of AA by Mo (VI)/IONPs biosensors:

The Influence of pH on the oxidation of ascorbic acid was studied at several pH values from 1 to 5. The absorbance of the blue complex formed by the oxidation of ascorbic acid by molybdate is measured by using UV-Vis spectrophotometer. The obtained absorbance at different pH values is summarized in Table III -7. It was found that the optimum pH condition is at pH=3 (Figure III-9). Thus, we selected this value as optimum values of colorimetric assay to simplify the AA detection process and prevent unnecessary influence.

The catalytic activity of the Fe_3O_4 NPs highly depends on the buffer pH used. As depicted in Table (3-9), the Fe_3O_4 NPs exhibits relatively high to catalyse the reaction of AA by molybdenum in medium acidic media, while in neutral media the activity turns to be very weak. Since the maximum absorbance is obtained at pH 3.0, a buffer with pH 3.0 is employed in the following study.

To confirm the stability of Magnetite NPs-Mo system, there were performed at different pH. As shown in Fig. Magnetite NPs exhibited a high catalytic activity at pH = 3. During detecting AA, the reaction conditions at 95 °C and pH 3.0 is suitable to obtain the highest catalytic activity for by Mo (VI)/IONPs biosensors. Higher and lower acidic condition may induce the decomposition of Mo, which reduces the catalytic activity.

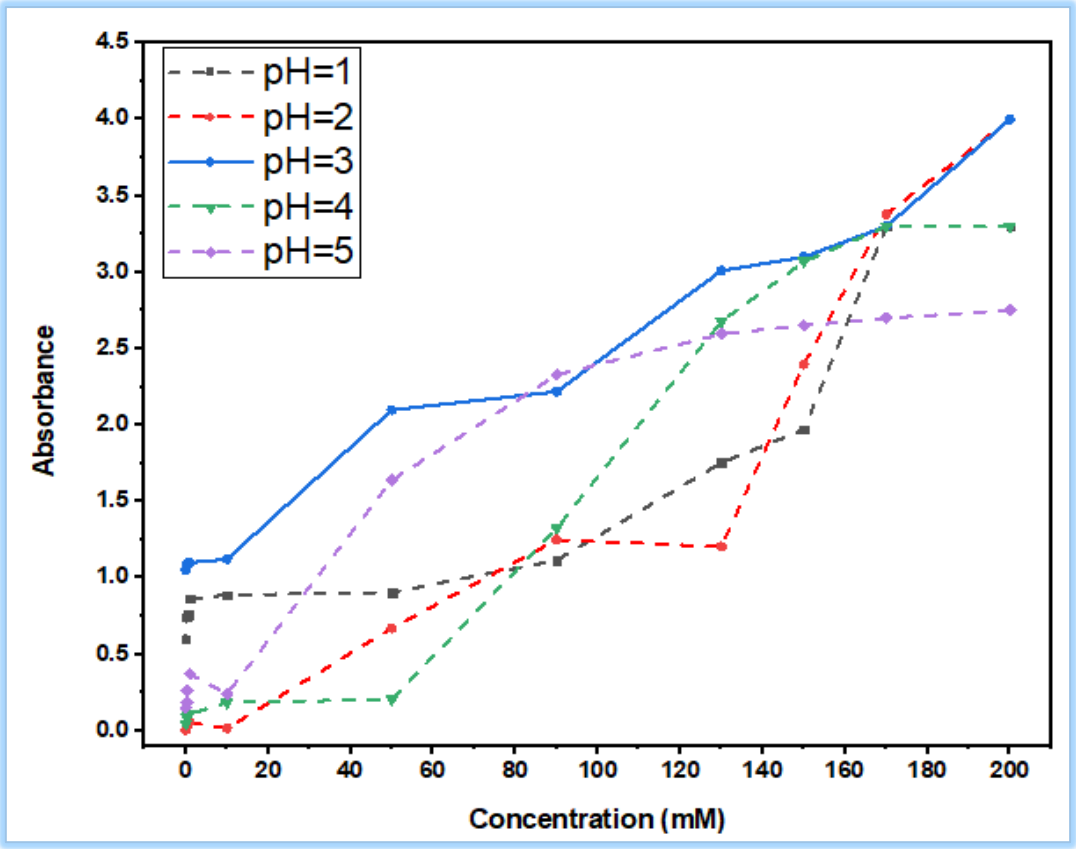

Figure III.9: Effect of pH on the oxidation of AA by Mo (VI)/IONPs biosensors at room Temperature at various pH's 1, 2, 3, 4 and 5.

Table III.7: value of absorbance obtained using UV-Vis for Effect of pH on Oxidation of Ascorbic Acid.

	pH =1	pH =2	pH =3	pH =4	pH =5
Concentration (mM)	**Abs1**	**Abs2**	**Abs3**	**Abs4**	**Abs5**
200	**3.3**	**4**	**4**	**3.3**	**2.750**
170	**3.3**	**3.379**	**3.3**	**3.3**	**2.700**
150	**1.969**	**2.397**	**3.1**	**3.07**	**2.650**
130	**1.753**	**1.204**	**3.01**	**2.678**	**2.596**
90	**1.116**	**1.249**	**2.218**	**1.325**	**2.329**
50	**0.905**	**0.671**	**2.098**	**0.205**	**1.638**
10	**0.889**	**0.016**	**1.122**	**0.185**	**0.240**
1	**0.863**	**0.058**	**1.1**	**0.111**	**0.373**
0.5	**0.758**	**0.035**	**1.093**	**0.107**	**0.263**
0.3	**0.745**	**0.041**	**1.086**	**0.089**	**0.186**

0.01	0.602	0.004	1.049	0.046	0.150

III-6-2- Colorimetric Detection of Ascorbic acid by Mo (VI)/IONPs biosensors

The Ascorbic acid detection test was carried out by colorimetric assay according to the principle of the following reaction:

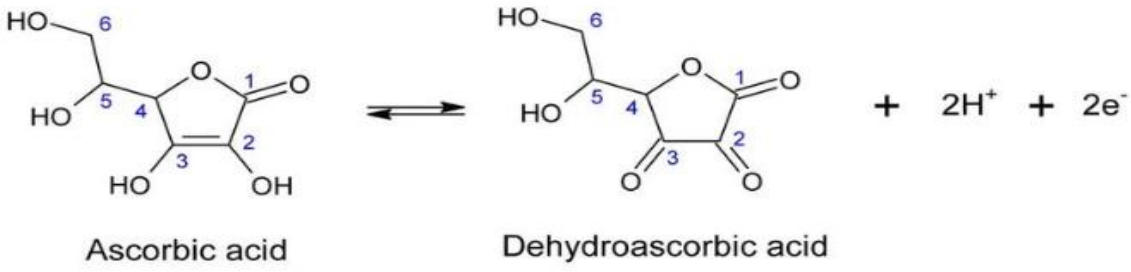

Figure III.10: Mechanism of oxidation of AA by Mo (VI)/Magnetite NPs in pH =3**.**

Ascorbic acid reacted with molybdate releasing blue-colored dehydroascorbic acid Figure (Figure III-10), the absorbance of which was measured by spectrophotometry at a wavelength of 820 nm.

The concentration of reduced ascorbic acid was determined by measuring the dehydroascorbic acid released into the reaction medium.

Owing to the AA can be oxidized from colorless to blue by Ammonium molybdate, a novel colorimetric assay was developed for detecting AA by Mo (VI)/IONPs biosensors in pH =3.

The Figure III-11 showed the spectrums of oxidation reaction of AA by Mo (VI)/ Magnetites biosensors in pH =3 after addition of 10 different concentrations of ascorbic acid in the range from 0.5-200 mM, in the spectral range of 400-900 nm FigureIII-11;III-12;III-13;III-14. It can be seen from the graphical data that absorption intensity increased with increasing the concentration of AA in all cases. Tube images for color degradation of AA are seen.

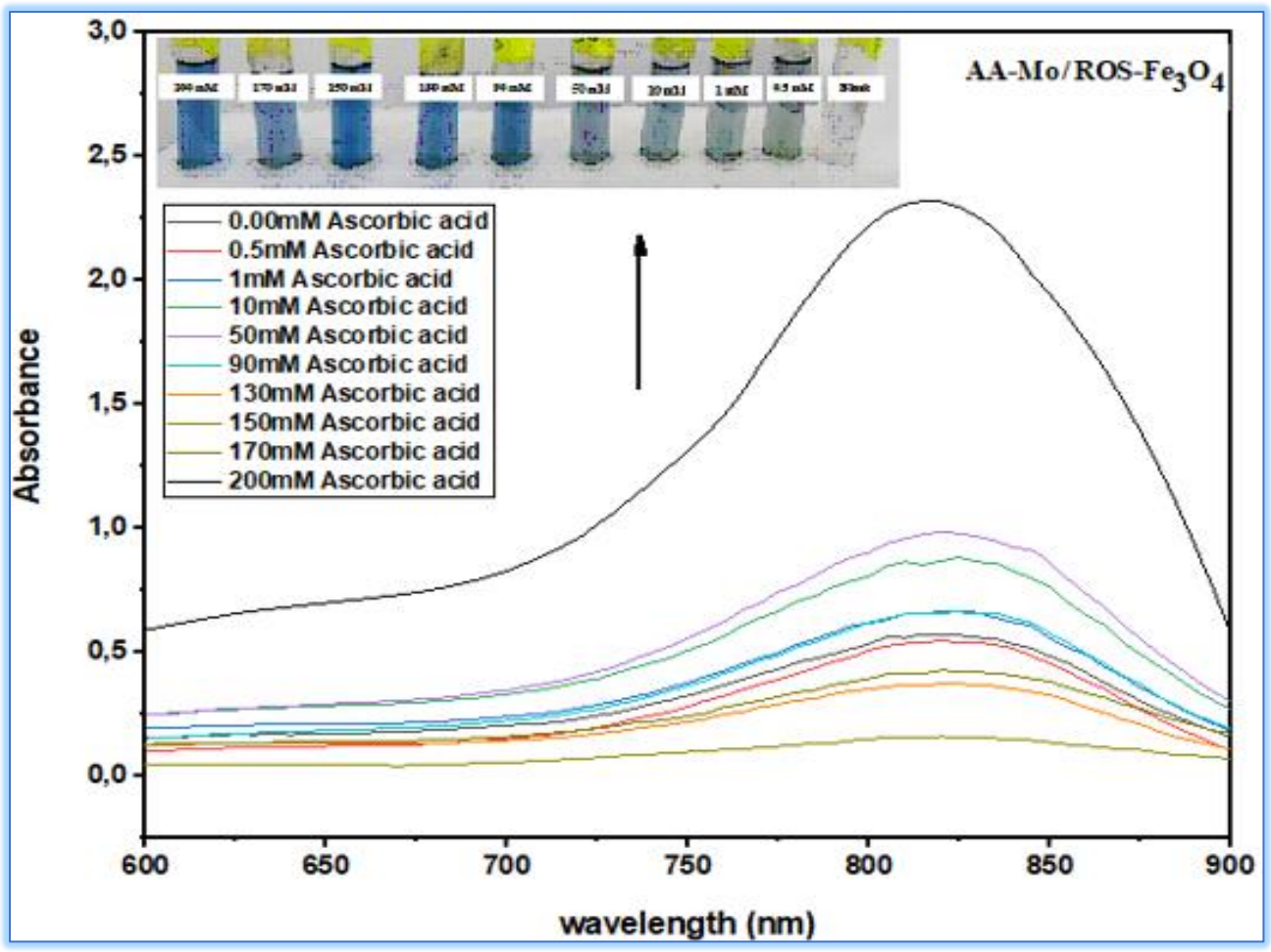

Figure III.11: Spectra of colorimetric detection of AA by Mo (VI)/ROS−Fe_3O_4 biosensor, in concentration range of 0.5-200 Mm.

Table III.8: Absorbance of detected ascorbic acid by Mo (VI)/ROS- $Fe3O_4$ biosensor.

Concentration(mM)	200	170	150	130	90	50	10	1	0.5
Absorbance	2.35	1	0.8	0.75	0.5	0.48	0.455	0.35	0.3

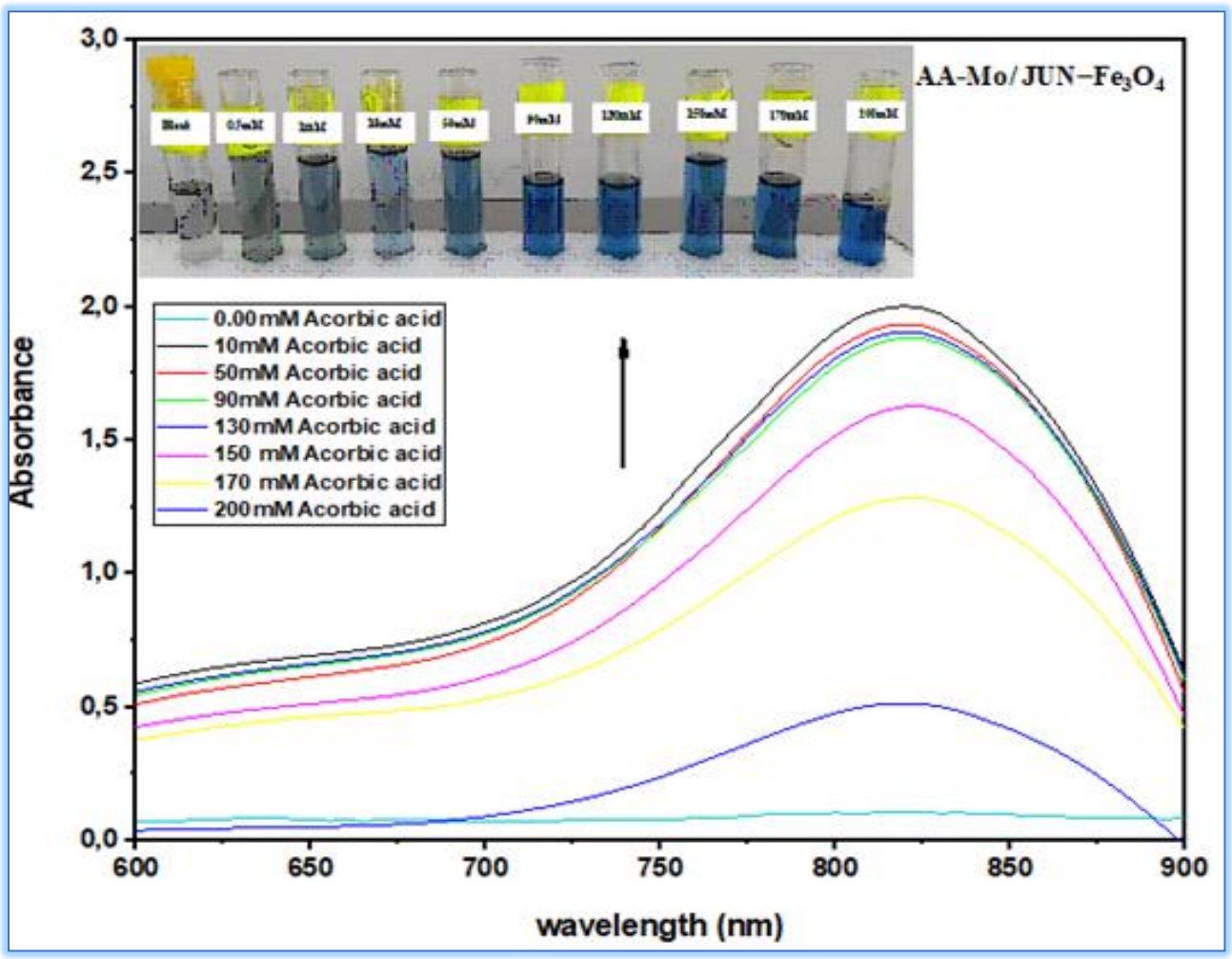

Figure III.12: Spectra of colorimetric detection of AA by Mo (VI)/JUN−Fe_3O_4 biosensor in concentration range of 0.5-200 Mm.

Table III.9: Absorbance of detected ascorbic acid by Mo (VI)/JUN- $Fe3O_4$ biosensor

Concentration (mM)	200	170	150	130	90	50	10	1	0.5
Asorbance	2.1	2	1.9	1.8	1	0.6	0.42	0.4	0.38

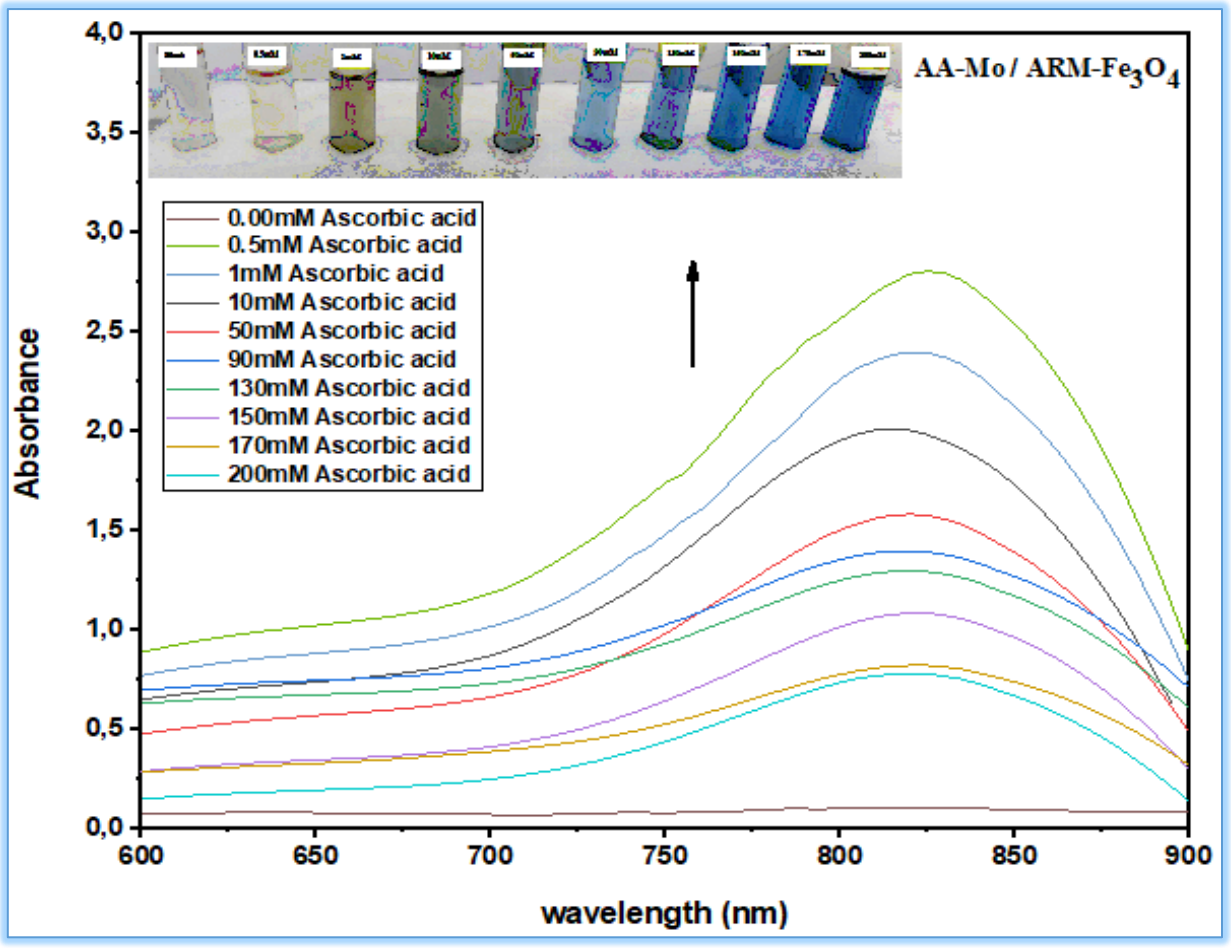

Figure III.13: Spectra of colorimetric detection of AA by Mo (VI)/ARM−Fe_3O_4 biosensor in concentration range 0.5-200 Mm.

Table III.10: Absorbance of detected ascorbic acid by Mo (VI)/ARM- $Fe3O_4$ biosensor

Concentration (mM)	200	170	150	130	90	50	10	1	0.5
Absorbance	2.8	2.5	2.2	1.6	1.45	1.4	1.2	0.9	0.6

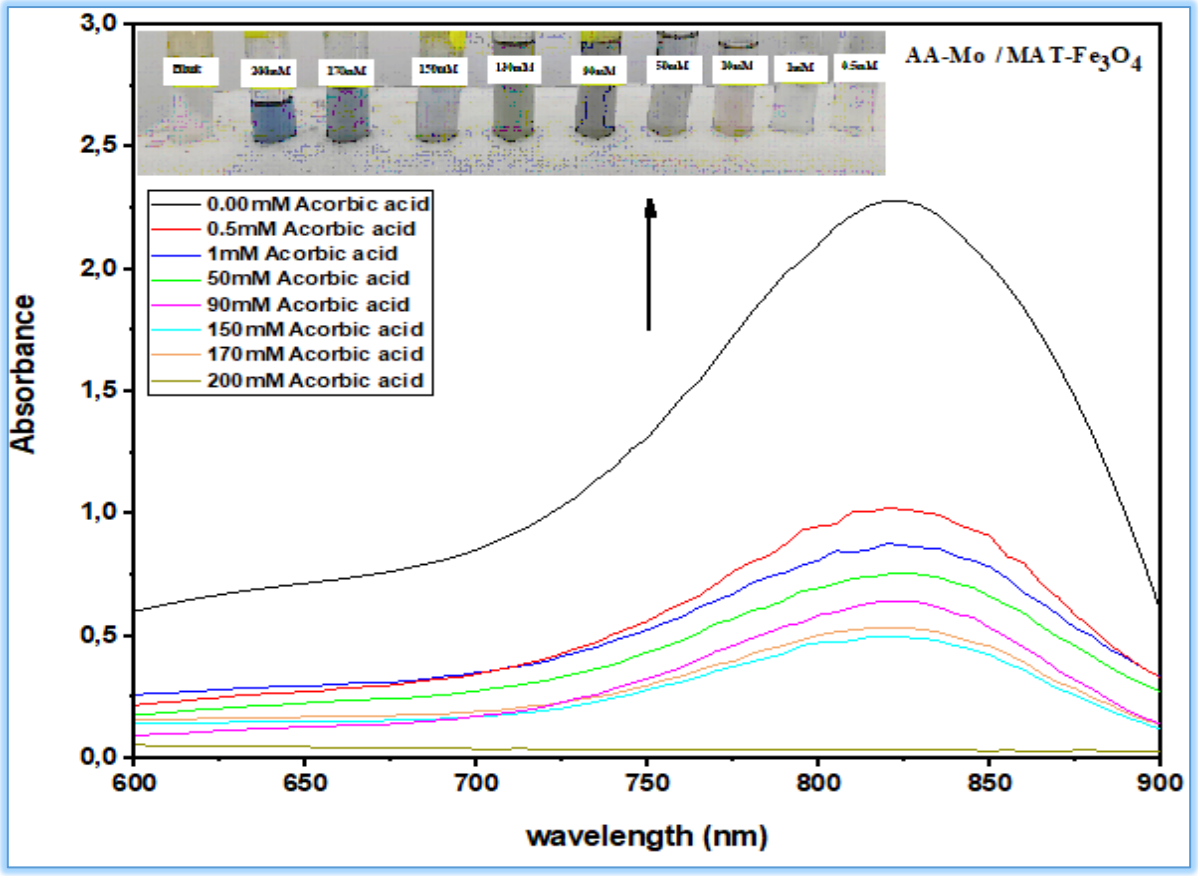

Figure III.14: Spectra of colorimetric detection of AA by Mo (VI)/MAT−Fe_3O_4, in concentration ranges from 0.5-200 Mm.

Table III.11: Absorbance of detected ascorbic acid by Mo (VI)/MAT- $Fe3O_4$ biosensor

Concentration(mM)	200	170	150	130	90	50	10	1	0.5
Absorbance	2.2	1.3	1	0.8	0.7	0.68	0.345	0.34	0.33

III-7- Study of linearity range and the calcul of LOD and LOQ

III-7-1- Calculation of the limit of detection (LOD)

The Limit of Detection (LOD) is the lowest concentration of the analyte in a sample that can be detected. Its value is calculated by comparing three times the standard deviation of a response to the smallest detected content.

The detection limit is calculated according to a noise/signal ratio = 3, the following equation:

$$LOD = (3 \times SD)/slope$$

Where, SD is the standard deviation, Slope is the slope of the linear curve.

The limit of colorimetric detection based on Mo(VI)/Magnetite NPs for AA detection are show in the Table III.12.

III.7.2 Calculation of the limit of quantification (LOQ)

Limit of quantification (LOQ) is the lowest concentration in a sample that has been accurately determined under specific conditions. The limit of quantification is determined from the standard deviation corresponding to several repeated measurements.

III.7.3 Calculation of the limit of quantity (LOQ)

The limit of quantification (LOQ) is calculated according to the following equation:

$$LOQ=(10 \times SD)/slope$$

Where, SD is the standard deviation, Slope is the slope of the linear curve.

The minimum amount of Mo(VI)/Magnetite NPs for AA detection were the results are shows in the table ().

Table III.12: LOD and LOQ data of AA Colorimetric Assay by Mo (VI)/IONPs

N.S	A	SD	LOD (mmol.L $^{-1}$)	LOQ (mmol.L^{-1})
AA- Mo(VI)/JUN−Fe_3O_4	**0.00365**	**0.0005718**	**0.47**	**1.566**
AA-Mo(VI)/MAT−Fe_3O_4	**0.00371**	**0.0005317**	**0.43**	**1.4315**
AA- Mo(VI)/ROS−Fe_3O_4	**0.00438**	**0.0005402**	**0.37**	**1.2333**
AA-Mo(VI)/ARM−Fe_3O_4	**0.01365**	**0.001456**	**0.32**	**1.666**

It is shown from FigureIII.14 that the range of linearity of (nano) between 0.5 to 10 mM

It is shown from FigureIII.15 that the range of linearity of (nano) is: Expression on a straight line

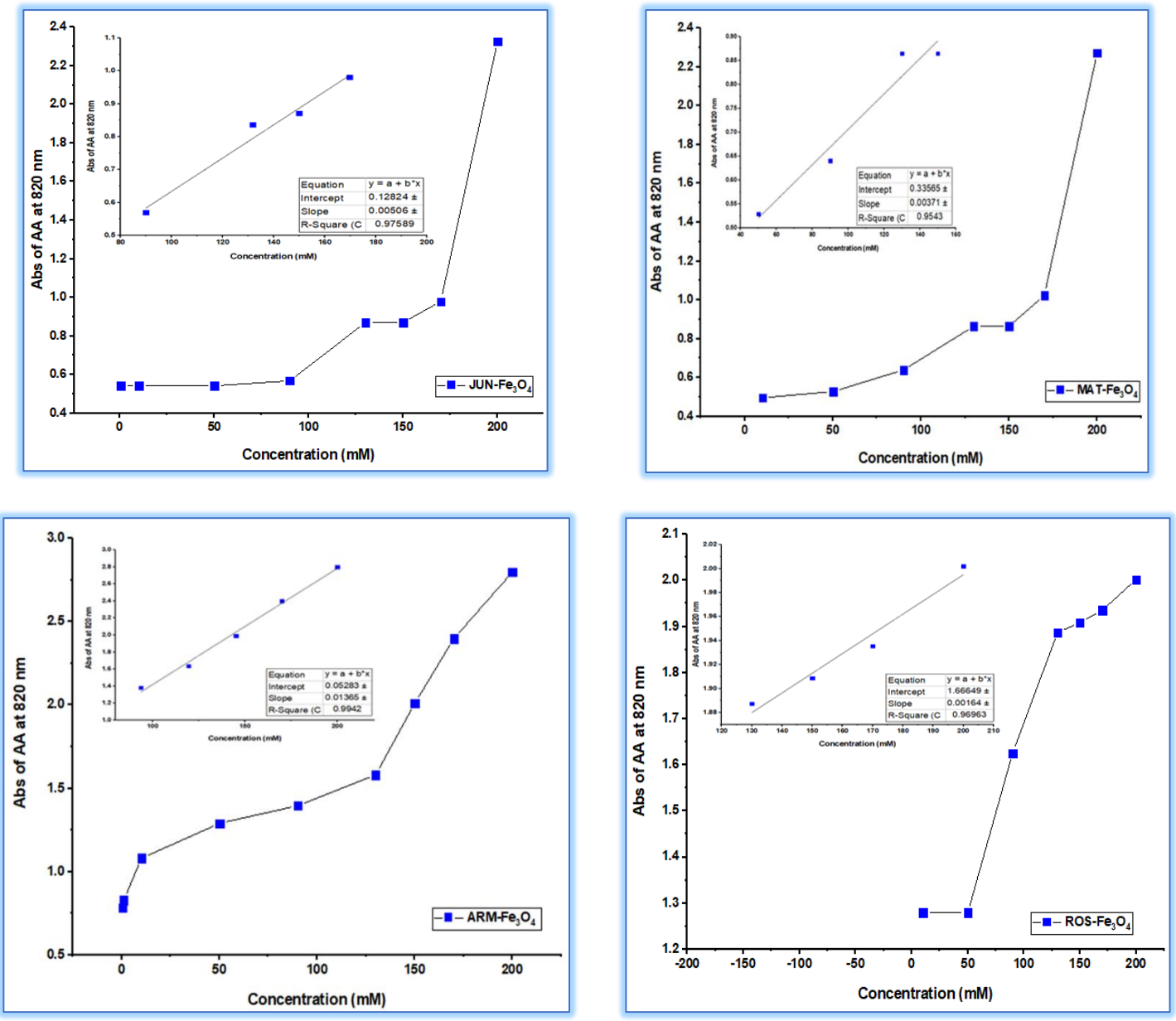

Figure III.15: viriation of the absorbance of oxidized aa by mo (vi)/magnetite biosensors at 820 nm with concentration ranges from 0.5-200 mm.

According to the with increasing AA cplots showen in FIGURE III.15, it is remarked that the absorbance at 820 nm increases with the increasing AA concentration and reached to its maximum values at 200mM. This indicates an improvement in AA oxidation reaction efficiency in the presence of iron nanoparticles as a catalyst. As seen in Fig. 5, the linear correlation was quite good (R^2=0.95 to 0.99),

In this study, a simple comparison between the JUN−Fe3O4, MAT−Fe3O4, ROS−Fe3O4, and ARM−Fe_3O_4 indicated that this ARM−Fe3O4 catalyst exhibited higher catalytic response for the detection of AA by Mo (VI)/IONPs biosensor, then ROS−Fe3O4 biosensor, next MAT−Fe3O4 biosensor, and finally JUN−Fe3O4 biosensor.

Ahmouda et al. studied the acidity of the four magnetite NPs samples via Bronstand and Lewis acid sites densities. They found that the acidity of mediating plants extracts of Artemisia herba-alba. (L), Rosemarinus officinalis. (L), Matricaria Pubescens (L), and Juniperus Phoenicia. (L), which were respectively 5.25, 5.05, 4.63, and 3.69 showed a main impact on the densities of Bronsted and Lewis acid sites located the four surfaces. They reported that Bronsted acid site density was lowest on ARM−Fe_3O_4, then ROS − Fe_3O_4, next MAT − Fe_3O_4, and finally JUN − Fe_3O_4 NPs. This may justify our finding herein the highest selectivity of ARM−Fe_3O_4 to AA molecules. AA molecules are acidic which make them more attractive (sensible) to less acidic surface such as ARM−Fe_3O_4, then ROS − Fe_3O_4, next MAT − Fe_3O_4, and finally JUN − Fe_3O_4 NPs.

III-8- Study of interference of different interferents on colorimetric detection of AA by by Mo (VI)/IONPs biosensors

The Influence of different interferents on the oxidation of ascorbic acid was investigated by adding different amounts of salts KCl, $CaCl_2$ and $CuCl_2$ as shown in Figure III-16.

The recovery (%) of AA in the presence of KCl, $CaCl_2$ and $CuCl_2$ is calculated by using the following equation:

$$\textbf{Recovery}\ (\%) = \frac{\textbf{Abs of interf} * \textbf{100}}{\textbf{Abs of AA}}$$

Where;

Abs_{AA}: is the absorbance of AA at 820 nm without the presence of the interferent.

Abs_{interf}: is the absorbance of AA at 820 nm with the presence of the interferent.

Figure III.17 show that the measured change in AA absorbance in the presence of the three types of interferents is insignificant, in all cases. This reveals the high selectivity of the four magnetite NPs to AA.

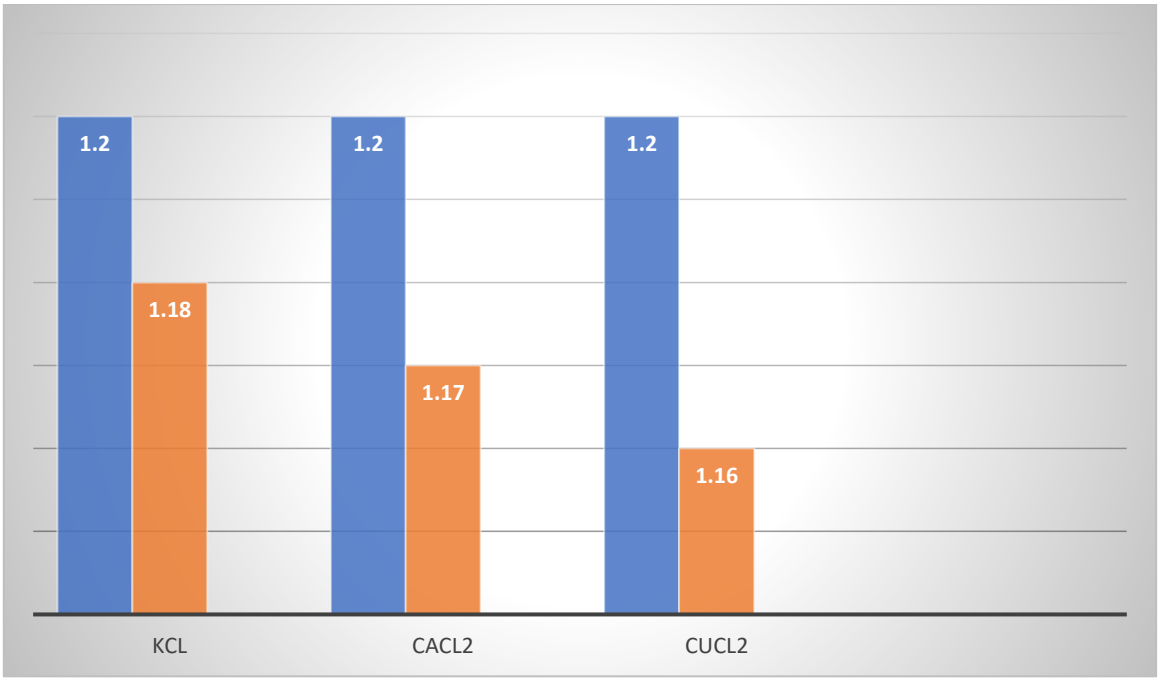

Figure III.16: Influence of the interferents on AA (10 mM) absorbance at 820 nm in the colorimetric detection of AA by Mo (VI)/ARM-Fe_3O_4 biosensor

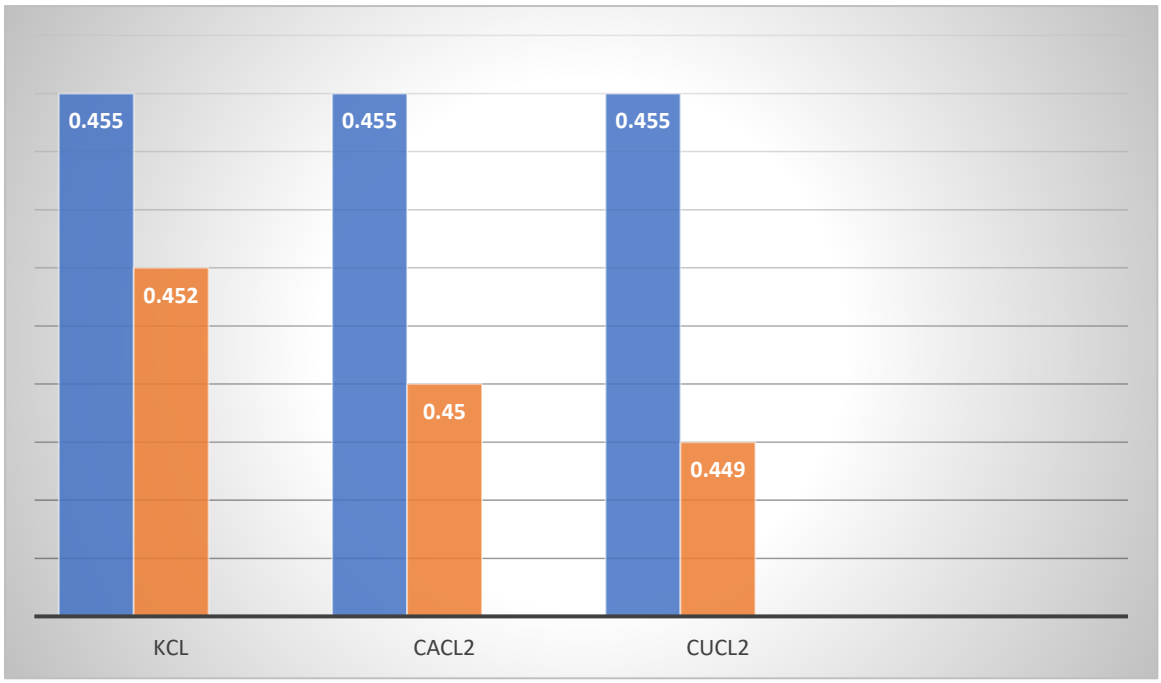

Figure III.17: Influence of the interferents on AA (10 mM) absorbance at 820 nm in the colorimetric detection of AA by Mo (VI)/ROS-Fe_3O_4 biosensor

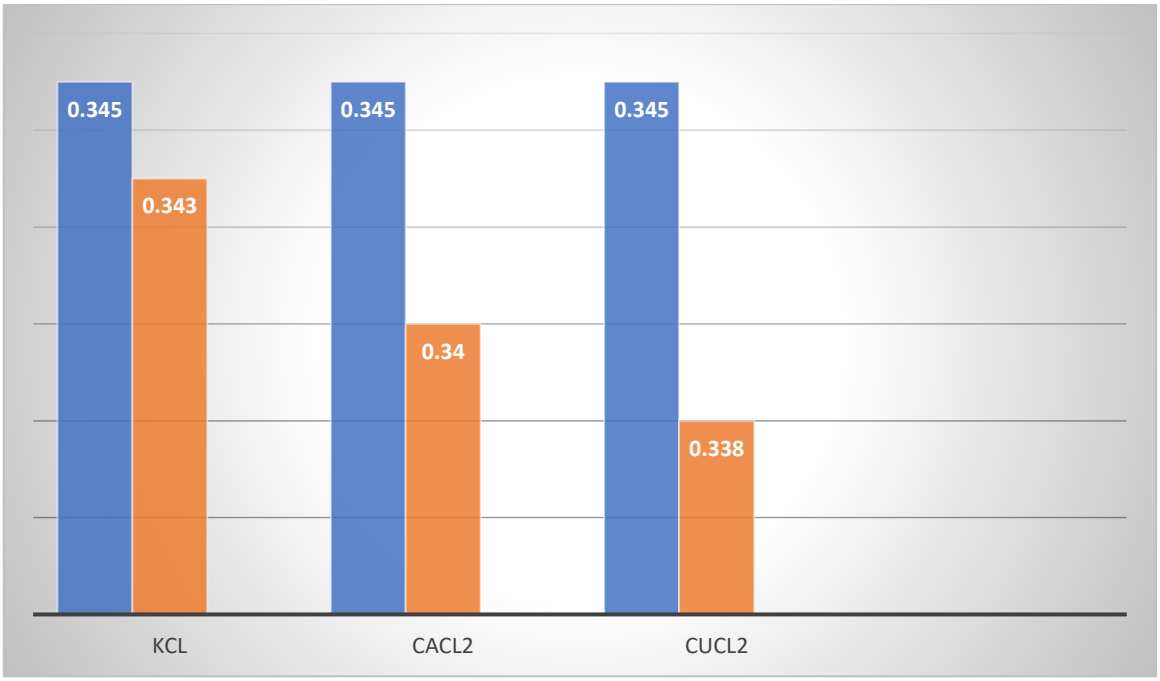

Figure III.18: Influence of the interferents on AA (10 mM) absorbance at 820 nm in the colorimetric detection of AA by Mo (VI)/MAT-Fe_3O_4 biosensor

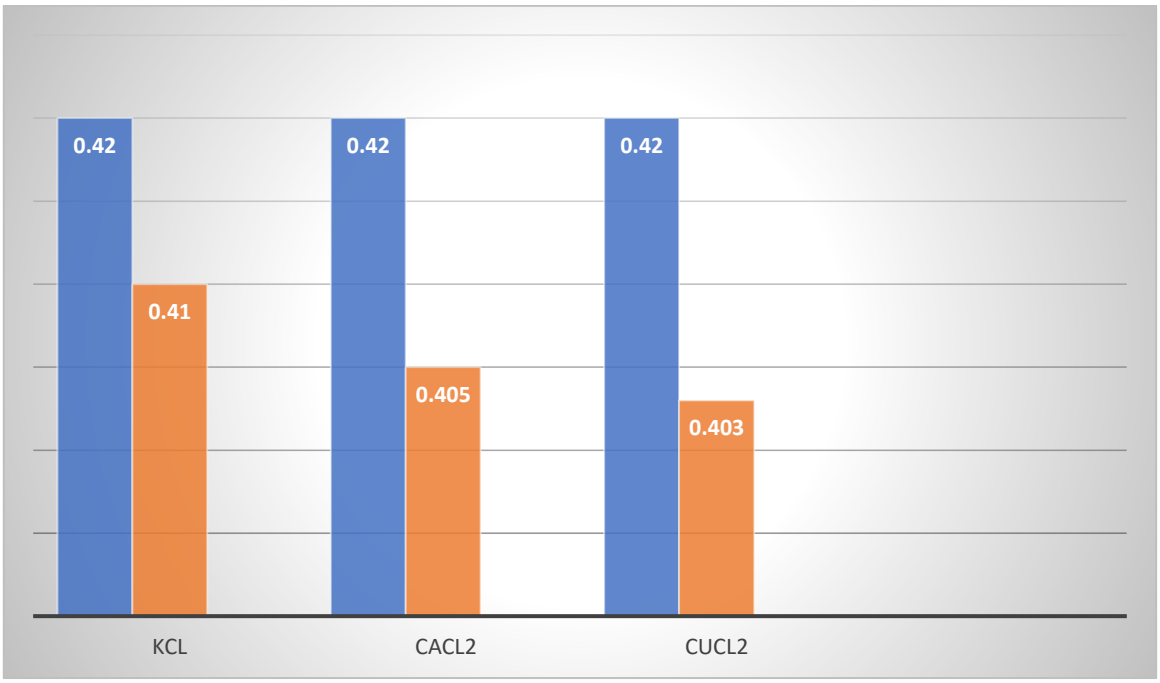

Figure III.19: Influence of the interferents on AA (10 mM) absorbance at 820 nm in the colorimetric detection of AA by Mo (VI)/JUN-Fe_3O_4 biosensor

Table III.14: Recovery (%) of AA by Mo (VI)/Fe_3O_4 biosensors in the presence of different interferents

Biosensor / Interferents	Mo (VI)/ARM-Fe_3O_4	Mo (VI)/ROS-Fe_3O_4	Mo (VI)/MAT-Fe_3O_4	Mo (VI)/JUN-Fe_3O_4
KCl	**98.33**	**98.34**	**97**	**98.78**
$CuCl_2$	**97.85**	**98.01**	**96.42**	**98.55**
$CaCl_2$	**96.66**	**98.00**	**96.40**	**97.97**

This Table shows us that the measured change in AA absorption (recovery %) in the presence of the three types of interfering elements is insignificant in all cases. This reveals the high selectivity of the four Mo (VI)/magnetite biosensors for detection AA.

III-9- Conclusion

This study developed and evaluated four biosensors which are: Mo (VI)/ARM-Fe_3O_4, Mo (VI)/ROS- Fe_3O_4, Mo (VI)/MAT- Fe_3O_4, and Mo (VI)/JUN- Fe_3O_4 for the colorimetric detection of ascorbic acid, aiming to enhance food security. Ascorbic acid was oxidized with ammonium molybdate at 95 °C for 1 hour, forming a blue complex with absorbance measured at 820 nm. The optimal pH for detection was found to be 3. Among the biosensors, Mo (VI)/ARM- Fe_3O_4 showed the highest sensitivity, followed by Mo (VI)/ROS- Fe_3O_4, Mo (VI)/MAT- Fe_3O_4 and Mo (VI)/JUN- Fe_3O_4.

The limits of detection (LOD) and quantification (LOQ) for each biosensor were calculated, with Mo (VI)/ARM- Fe_3O_4 demonstrating the lowest LOD and LOQ, indicating superior sensitivity. Interference studies with CaCl2, CuCl2, and KCl showed no significant impact on ascorbic acid detection. In conclusion, the Mo (VI)/ARM- Fe_3O_4 biosensor was the most effective, providing a simple, rapid, and highly sensitive method for detecting ascorbic acid, thus ensuring food quality and safety and enhancing food security.

GENERAL CONCLUSION

This study focused on the development and evaluation of four different biosensor Mo (VI)/ARM-Fe_3O_4, Mo (VI)/ROS- Fe_3O_4, Mo (VI)/MAT- Fe_3O_4 and Mo (VI)/JUN-Fe_3O_4 for the colorimetric detection of ascorbic acid, a key spoilage compound in food products. The objective was to create an effective, sensitive, and rapid method for detecting ascorbic acid to enhance food security.

The experiments involved oxidizing ascorbic acid with ammonium molybdate at 95 °C for 1 hour, resulting in the formation of a blue complex whose absorbance was measured at 820 nm. The impact of pH on the detection efficiency was studied, with the optimal pH found to be 3. Among the biosensors tested, Mo (VI)/ARM- Fe_3O_4 exhibited the highest sensitivity in detecting ascorbic acid, followed by Mo (VI)/ROS-Fe_3O_4, Mo (VI)/MAT-Fe_3O_4, and Mo (VI)/JUN- Fe_3O_4.

The limits of detection (LOD) and limits of quantification (LOQ) were calculated for each biosensor. The results indicated that Mo (VI)/ARM-Fe_3O_4 had the lowest LOD and LOQ, highlighting its superior sensitivity. Additionally, the study assessed the potential interference from $CaCl_2$, $CuCl_2$, and KCl, demonstrating that these compounds did not significantly interfere with the detection of ascorbic acid.

In conclusion, the Mo (VI)/ARM- Fe_3O_4 biosensor proved to be the most effective, offering a simple, rapid, and highly sensitive method for the colorimetric detection of ascorbic acid. This advancement provides a valuable tool for ensuring food quality and safety, contributing significantly to the control of spoilage compounds and enhancing food security.

LIST OF REFERENCE

[1]. Berry, E.M., et al., Food security and sustainability: can one exist without the other? Public health nutrition, 2015. **18**(13): p. 2293-2302.

[2]. Savov, A. and G. Kouzmanov, Food quality and safety standards at a glance. Biotechnology & Biotechnological Equipment, 2009. **23**(4): p. 1462-1468.

[3]. Teshome, E., et al., Potentials of natural preservatives to enhance food safety and shelf life: A review. The Scientific World Journal, 2022. **2022**.

[4]. Abdelhamid, A.G. and N.K. El-Dougdoug, Controlling foodborne pathogens with natural antimicrobials by biological control and antivirulence strategies. Heliyon, 2020. **6**(9).

[5]. Iqbal, K., A. Khan, and M. Khattak, Biological significance of ascorbic acid (vitamin C) in human health-a review. Pakistan Journal of Nutrition, 2004. **3**(1): p. 5-13.

[6]. Bsoul, S.A. and G.T. Terezhalmy, Vitamin C in health and disease. J Contemp Dent Pract, 2004. **5**(2): p. 1-13.

[7]. Kang, H., et al., Nanoparticles for biosensors, in Optical biosensors. 2008, Elsevier. p. 583-621.

[8]. Fernandes, G.M., et al., Novel approaches for colorimetric measurements in analytical chemistry–A review. Analytica Chimica Acta, 2020. **1135**: p. 187-203.

[9]. Neethirajan, S., et al., Biosensors for sustainable food engineering: challenges and perspectives. Biosensors, 2018. **8**(1): p. 23.

[10]. Mittu, B., et al., Ascorbic acid, in Nutraceuticals and Health Care. 2022, Elsevier. p. 289-302.

[11]. Pathy, K., Process for preparation of vitamin C and method for determination of vitamin C in tablets. SF J Chem Res, 2018. **2**(1): p. 2.

[12]. Padayatty, S.J., et al., Vitamin C as an antioxidant: evaluation of its role in disease prevention. Journal of the American college of Nutrition, 2003. **22**(1): p. 18-35.

[13]. Afolalu, S.A., et al. Advances in Nanotechnology and Nanoparticles in the 21st Century–An Overview. in Proceedings of the 3rd African International Conference on Industrial Engineering and Operations Management, Nsukka, Nigeria. 2022.

[14]. Behera, A., Advanced Materials: An Introduction to Modern Materials Science. 2021: Springer Nature.

[15]. Murray, J.W., Iron oxides, in Marine minerals. 1979, Mineralogical Society of America Washington, DC. p. 47-98.

[16]. Guo, H. and A.S. Barnard, Naturally occurring iron oxide nanoparticles: morphology, surface chemistry and environmental stability. Journal of Materials Chemistry A, 2013. **1**(1): p. 27-42.

[17]. Ahmed, I., et al., The importance of iron oxides in natural environment and significance of its nanoparticles application. Nanomaterials for Environmental Applications and their Fascinating Attributes, 2018. **2**: p. 218.

[18]. Ajinkya, N., et al., Magnetic iron oxide nanoparticle (IONP) synthesis to applications: present and future. Materials, 2020. **13**(20): p. 4644.

[19]. Alphandéry, E., Bio-synthesized iron oxide nanoparticles for cancer treatment. International journal of pharmaceutics, 2020. **586**: p. 119472.

[20]. Tadic, M., et al., Magnetic properties of hematite (α-Fe2O3) nanoparticles prepared by hydrothermal synthesis method. Applied Surface Science, 2014. **320**: p. 183-187.

[21]. Avram, A., et al., Synthesis and characterization of γ-Fe2O3 nanoparticles for applications in magnetic hyperthermia. Synthesis, 2011. **10**(P151): p. 1.

[22]. Darezereshki, E., Synthesis of maghemite (γ-Fe2O3) nanoparticles by wet chemical method at room temperature. Materials Letters, 2010. **64**(13): p. 1471-1472.

[23]. Dar, M.I. and S. Shivashankar, Single crystalline magnetite, maghemite, and hematite nanoparticles with rich coercivity. RSC Advances, 2014. **4**(8): p. 4105-4113.

[24]. Ali, A., et al., Synthesis, characterization, applications, and challenges of iron oxide nanoparticles. Nanotechnology, science and applications, 2016: p. 49-67.

[25]. Yusefi, M., K. Shameli, and A.F. Jumaat, Preparation and properties of magnetic iron oxide nanoparticles for biomedical applications: A brief review. Journal of Advanced Research in Materials Science, 2020. **75**(1): p. 10-18.

[26]. Abenojar, E.C., et al., Structural effects on the magnetic hyperthermia properties of iron oxide nanoparticles. Progress in Natural Science: Materials International, 2016. **26**(5): p. 440-448.

[27]. Tiwari, J.N., R.N. Tiwari, and K.S. Kim, Zero-dimensional, one-dimensional, two-dimensional and three-dimensional nanostructured materials for advanced electrochemical energy devices. Progress in Materials Science, 2012. **57**(4): p. 724-803.

[28]. Tang, Z. and N.A. Kotov, One-dimensional assemblies of nanoparticles: preparation, properties, and promise. Advanced Materials, 2005. **17**(8): p. 951-962.

[29]. Chimene, D., D.L. Alge, and A.K. Gaharwar, Two-dimensional nanomaterials for biomedical applications: emerging trends and future prospects. Advanced Materials, 2015. **27**(45): p. 7261-7284.

[30]. Leventis, N., Three-dimensional core-shell superstructures: mechanically strong aerogels. Accounts of chemical research, 2007. **40**(9): p. 874-884.

[31]. Ijaz, I., et al., Detail review on chemical, physical and green synthesis, classification, characterizations and applications of nanoparticles. Green Chemistry Letters and Reviews, 2020. **13**(3): p. 223-245.

[32]. Wang, N., et al., Synthesis methods of functionalized nanoparticles: a review. Bio-Design and Manufacturing, 2021. **4**(2): p. 379-404.

[33]. El-Khawaga, A.M., A. Zidan, and A.I. Abd El-Mageed, Preparation methods of different nanomaterials for various potential applications: A review. Journal of Molecular Structure, 2023. **1281**: p. 135148.

[34]. Zheng, K. and P.S. Branicio, Synthesis of metallic glass nanoparticles by inert gas condensation. Physical Review Materials, 2020. **4**(7): p. 076001.

[35]. Deng, Y., et al., Physical vapor deposition technology for coated cutting tools: A review. Ceramics International, 2020. **46**(11): p. 18373-18390.

[36]. Nyabadza, A., M. Vazquez, and D. Brabazon, A review of bimetallic and monometallic nanoparticle synthesis via laser ablation in liquid. Crystals, 2023. **13**(2): p. 253.

[37]. Jiang, Z., et al., Progress in laser ablation and biological synthesis processes:“Top-Down” and “Bottom-Up” approaches for the green synthesis of Au/Ag nanoparticles. International Journal of Molecular Sciences, 2022. **23**(23): p. 14658.

[38]. Bokov, D., et al., Nanomaterial by sol-gel method: synthesis and application. Advances in Materials Science and Engineering, 2021. **2021**: p. 1-21.

[39]. Parashar, M., V.K. Shukla, and R. Singh, Metal oxides nanoparticles via sol–gel method: a review on synthesis, characterization and applications. Journal of Materials Science: Materials in Electronics, 2020. **31**(5): p. 3729-3749.

[40]. Mohan, S., et al., Hydrothermal synthesis and characterization of Zinc Oxide nanoparticles of various shapes under different reaction conditions. Nano Express, 2020. **1**(3): p. 030028.

[41]. Bahrulolum, H., et al., Green synthesis of metal nanoparticles using microorganisms and their application in the agrifood sector. Journal of Nanobiotechnology, 2021. **19**: p. 1-26.

[42]. Tsekhmistrenko, S., et al., Bacterial synthesis of nanoparticles: A green approach. Biosystems Diversity, 2020. **28**(1): p. 9-17.

[43]. Salem, S.S. and A. Fouda, Green synthesis of metallic nanoparticles and their prospective biotechnological applications: an overview. Biological trace element research, 2021. **199**(1): p. 344-370.

[44]. Kumari, S., et al., A comprehensive review on various techniques used for synthesizing nanoparticles. Journal of Materials Research and Technology, 2023.

[45]. Vijayaram, S., et al., Applications of green synthesized metal nanoparticles—a review. Biological Trace Element Research, 2024. **202**(1): p. 360-386.

[46]. Shafey, A.M.E., Green synthesis of metal and metal oxide nanoparticles from plant leaf extracts and their applications: A review. Green Processing and Synthesis, 2020. **9**(1): p. 304-339.

[47]. Bandeira, M., et al., Green synthesis of zinc oxide nanoparticles: A review of the synthesis methodology and mechanism of formation. Sustainable Chemistry and Pharmacy, 2020. **15**: p. 100223.

[48]. Nadeem, M., et al., A review of microbial mediated iron nanoparticles (IONPs) and its biomedical applications. Nanomaterials, 2021. **12**(1): p. 130.

[49]. Alphandéry, E., Iron oxide nanoparticles for therapeutic applications. Drug discovery today, 2020. **25**(1): p. 141-149.

[50]. Góral, D., et al., Application of iron nanoparticle-based materials in the food industry. Materials, 2023. **16**(2): p. 780.

[51]. Ganachari, S.V., et al., Green nanotechnology for biomedical, food, and agricultural applications. 2019.

[52]. Jin, R., The impacts of nanotechnology on catalysis by precious metal nanoparticles. Nanotechnology Reviews, 2012. **1**(1): p. 31-56.

[53]. Zhang, Y., et al., Nano-gold catalysis in fine chemical synthesis. Chemical Reviews, 2012. **112**(4): p. 2467-2505.

[54]. Kumar, P., et al., Nanotechnology and its challenges in the food sector: a review. Materials Today Chemistry, 2020. **17**: p. 100332.

[55]. Singh, R., et al., Future of nanotechnology in food industry: Challenges in processing, packaging, and food safety. Global Challenges, 2023. **7**(4): p. 2200209.

[56]. Nikolic, M.V., et al., Metal oxide nanoparticles for safe active and intelligent food packaging. Trends in Food Science & Technology, 2021. **116**: p. 655-668.

[57]. Garcia, C.V., G.H. Shin, and J.T. Kim, Metal oxide-based nanocomposites in food packaging: Applications, migration, and regulations. Trends in food science & technology, 2018. **82**: p. 21-31.

[58]. Kalpana, V. and V.D. Rajeswari, Biosynthesis of metal and metal oxide nanoparticles for food packaging and preservation: a green expertise, in Food biosynthesis. 2017, Elsevier. p. 293-316.

[59]. Galstyan, V., et al., Metal oxide nanostructures in food applications: Quality control and packaging. Chemosensors, 2018. **6**(2): p. 16.

[60]. !!! INVALID CITATION !!!

[61]. Bunaciu, A.A., E.G. UdriŞTioiu, and H.Y. Aboul-Enein, X-ray diffraction: instrumentation and applications. Critical reviews in analytical chemistry, 2015. **45**(4): p. 289-299.

[62]. Fatimah, S., et al., How to calculate crystallite size from x-ray diffraction (XRD) using Scherrer method. ASEAN Journal of Science and Engineering, 2022. **2**(1): p. 65-76.

[63]. Ermrich, M. and D. Opper, XRD for the analyst: Getting acquainted with the principles. 2013: PANalytical.

[64]. Mohammed, A. and A. Abdullah. Scanning electron microscopy (SEM): A review. in Proceedings of the 2018 International Conference on Hydraulics and Pneumatics—HERVEX, Băile Govora, Romania. 2018.

[65]. Inkson, B.J., Scanning electron microscopy (SEM) and transmission electron microscopy (TEM) for materials characterization, in Materials characterization using nondestructive evaluation (NDE) methods. 2016, Elsevier. p. 17-43.

[66]. Michler, G.H., Scanning Electron Microscopy (SEM). 2008, Springer.

[67]. Friese, M.A., S. Banerjee, and P.J. Mangin, FT-IR Spectroscopy. Surface analysis of paper, 2020: p. 119-141.

[68]. Crupi, V., et al., FT-IR spectroscopy: a powerful tool in pharmacology. Journal of pharmaceutical and biomedical analysis, 2002. **29**(6): p. 1149-1152.

[69]. Amit, S.K., et al., A review on mechanisms and commercial aspects of food preservation and processing. Agriculture & Food Security, 2017. **6**: p. 1-22.

[70]. Rawat, S., Food Spoilage: Microorganisms and their prevention. Asian journal of plant science and Research, 2015. **5**(4): p. 47-56.

[71]. Sonwani, E., et al., An artificial intelligence approach toward food spoilage detection and analysis. Frontiers in Public Health, 2022. **9**: p. 816226.

[72]. Szelenberger, R., et al., Application of Biosensors for the Detection of Mycotoxins for the Improvement of Food Safety. Toxins, 2024. **16**(6): p. 249.

[73]. Yarik. S, Moussous. L, Dégradation des polluants organiques par des catalyseurs de type pérovskite/TiO_2. Mémoire de Master, Université de Bejaïa (2016).

[74]. Khelifi. T, Synthèse et caractérisation des nanoparticules à base de $Bi_{1-x}Al_xFeO_3$. Application : capteur d'humidité. Mémoire de Master, université mouloud Mammeri – Tizi ouzou (2017).

[75]. Hammachi. S, Couches minces nanocristallines et texturées d'oxyde de Zinc préparées par Sol-Gel. Mémoire de Master, Université M'hamed Bougara - Boumerdès (2017).

[76]. Mohammadi, Z. and S.M. Jafari, Detection of food spoilage and adulteration by novel nanomaterial-based sensors. Advances in colloid and interface Science, 2020. **286**: p. 102297.

[77]. Malaysia, P., Food security: concepts and definitions. Journal of Community Health, 2010. **16**(2): p. 2.

[78]. Ramp, W., Complicating food security: Definitions, discourses, commitments. 2014.

[79]. Shaw, D.J., World food security. A History since, 1945.

[80]. Ehrlich, P.R., A.H. Ehrlich, and G.C. Daily, Food security, population and environment. Population and development review, 1993: p. 1-32.

[81]. Campaniello, D. and M. Sinigaglia, Wine spoiling phenomena, in The Microbiological Quality of Food. 2017, Elsevier. p. 237-255.

[82]. Amin, R.A., Effect of bio preservation as a modern technology on quality aspects and microbial safety of minced beef. Global Journal of Biotechnology & Biochemistry, 2012. **7**(2): p. 38-49.

[83]. in't Veld, J.H.H., Microbial and biochemical spoilage of foods: an overview. International journal of Food microbiology, 1996. **33**(1): p. 1-18.

[84]. Dainty, R.H., Chemical/biochemical detection of spoilage. International journal of food microbiology, 1996. **33**(1): p. 19-33.

[85]. Anastassakis, K., Vitamins: Definition and Types, in Androgenetic Alopecia From A to Z: Vol. 2 Drugs, Herbs, Nutrition and Supplements. 2022, Springer. p. 295-296.

[86]. Rucker, R.B. and J.G. Morris, The vitamins, in Clinical biochemistry of domestic animals. 1997, Elsevier. p. 703-739.

[87]. Svirbely, J.L. and A. Szent-Györgyi, The chemical nature of vitamin C. Biochemical Journal, 1932. **26**(3): p. 865.

[88]. Gibson, G.E., et al., Vitamin B1 (thiamine) and dementia. Annals of the New York Academy of Sciences, 2016. **1367**(1): p. 21-30.

[89]. Gram, L., et al., Food spoilage—interactions between food spoilage bacteria. International journal of food microbiology, 2002. **78**(1-2): p. 79-97.

[90]. Sahu, M. and S. Bala, Food processing, food spoilage and their prevention: An overview. International Journal of Life-Sciences Scientific Research, 2017. **3**(1): p. 753-759.

[91]. Yousef, A.E. and V. Balasubramaniam, Physical methods of food preservation. Food microbiology: Fundamentals and frontiers, 2012: p. 735-763.

[92]. Sen, M., Food chemistry: role of additives, preservatives, and adulteration. Food chemistry: the role of additives, preservatives and adulteration, 2021: p. 1-42.

[93]. Petruzzi, L., et al., Microbial spoilage of foods: Fundamentals, in The microbiological quality of food. 2017, Elsevier. p. 1-21.

[94]. López-Rubio, A., Bioactive food packaging strategies. Multifunctional and nanoreinforced polymers for food packaging, 2011: p. 460-482.

[95]. Moeini, A., et al., Edible polymers and secondary bioactive compounds for food packaging applications: Antimicrobial, mechanical, and gas barrier properties. Polymers, 2022. **14**(12): p. 2395.

[96]. Zhang, Y., et al., A review of the extraction and determination methods of thirteen essential vitamins to the human body: An update from 2010. Molecules, 2018. **23**(6): p. 1484.

[97]. Bürzle, M. and M.A. Hediger, Functional and physiological role of vitamin C transporters. Current topics in membranes, 2012. **70**: p. 357-375.

[98]. Levine, M., et al., Vitamin C pharmacokinetics in healthy volunteers: evidence for a recommended dietary allowance. Proceedings of the National Academy of Sciences, 1996. **93**(8): p. 3704-3709.

[99]. Hansen, S.N., P. Tveden-Nyborg, and J. Lykkesfeldt, Does vitamin C deficiency affect cognitive development and function? Nutrients, 2014. **6**(9): p. 3818-3846.

[100]. Malik, M., V. Narwal, and C. Pundir, Ascorbic acid biosensing methods: A review. Process Biochemistry, 2022. **118**: p. 11-23.

[101]. Wang, L., et al., A novel ratiometric electrochemical biosensor for sensitive detection of ascorbic acid. Sensors and Actuators B: Chemical, 2017. **242**: p. 625-631.

[102]. Chandra, S., et al., Mustard seeds derived fluorescent carbon quantum dots and their peroxidase-like activity for colorimetric detection of H2O2 and ascorbic acid in a real sample. Analytica chimica acta, 2019. **1054**: p. 145-156.

[103]. Li, R., et al., Molybdenum oxide nanosheets meet ascorbic acid: tunable surface plasmon resonance and visual colorimetric detection at room temperature. Sensors and Actuators B: Chemical, 2018. **259**: p. 59-63.

[104]. Li, S., et al., Gold nanoparticles based colorimetric probe for Cr (III) and Cr (VI) detection. Colloids and Surfaces A: Physicochemical and Engineering Aspects, 2017. **535**: p. 215-224.

[105]. Liu, Y. and X. Wang, Colorimetric speciation of Cr (III) and Cr (VI) with a gold nanoparticle probe. Analytical methods, 2013. **5**(6): p. 1442-1448.

[106]. Sui, N., et al., Colorimetric detection of ascorbic acid based on the trigger of gold nanoparticles aggregation by Cr (III) reduced from Cr (VI). Analytical Sciences, 2017. **33**(8): p. 963-967.

[107]. Shishehbore, M.R. and Z. Aghamiri, A highly sensitive kinetic spectrophotometric method for the determination of ascorbic acid in pharmaceutical samples. Iranian journal of pharmaceutical research: IJPR, 2014. **13**(2): p. 373.

[108]. Priego-Capote, F., Solid–liquid extraction techniques, in Analytical sample preparation with nano-and other high-performance materials. 2021, Elsevier. p. 111-130.

[109]. Ahmouda, K., et al., Plant extract FRAP effect on cation vacancies formation in greenly synthesized wüstite (FexO) nanoparticles: A new contribution. Sustainable Chemistry and Pharmacy, 2022. **25**: p. 100563.

[110]. Ahmouda, K., et al., The effect of mediating plant extract on the photocatalytic activity of different eco-friendly synthesized magnetite nanoparticles against cresol red photodegradation. Journal of Photochemistry and Photobiology A: Chemistry, 2024. **450**: p. 115442.